UNIVERSITY OF OKLAHOMA

GRADUATE COLLEGE

STEADY STATE PERMEABILITY MEASUREMENTS IN SHALES

A THESIS

SUBMITTED TO THE GRADUATE FACULTY

in partial fulfillment of the requirements for the

Degree of

MASTER OF SCIENCE

By

JYOTADITYA SINGH
Norman, Oklahoma
2018

STEADY STATE PERMEABILITY MEASUREMENTS IN SHALES

A THESIS APPROVED FOR THE
MEWBOURNE SCHOOL OF PETROLEUM AND GEOLOGICAL ENGINEERING

BY

_____
Dr. Carl H. Sondergeld, Chair

_____
Dr. Chandra S. Rai

_____
Dr. Deepak Devegowda

Acknowledgements

I would like to extend my sincere gratitude to my advisors Dr. Carl Sondergeld and Dr. Chandra Rai. Their guidance, support, counsel and critique have helped me to complete my thesis. I would also like to thank Dr. Deepak Devegowda for being the co-chair and providing valuable recommendations to improve the quality of this work.

I am also thankful to fellow students and colleagues at the Integrated Core Characterization Center and the petroleum engineering department who have helped immensely in conducting the experiments for this work, especially Bruce Spears, Gary Stowe, Rohit Bakshi, Shantanu Taneja, Son Thai Dang, Ankita Sinha and Ali Tinni.

My time at OU was made enjoyable in large part due to the many wonderful friends in Norman who have become a part of my life.

Finally, I wish to express my profound gratitude to my parents and sister, who provided unfailing support and encouragement and prayed for me throughout my tenure at OU.

Table of Contents

List of Tables

List of Figures

Abstract

Characterizing matrix permeability in shale formations is vital to determining the long term productivity of a reservoir as well as determining the optimal completion design. Permeability of shales lies in the nanodarcy (six orders of magnitude lower than conventional reservoir formations) range and the pore structure of these rocks is often complex, characterized by mixed wettability and presence of organics.

In this work, we find that the permeability of shales is dependent on the pore fluid used for estimation. Gas (nitrogen) and liquid (dodecane) permeability measurements carried out on the same core plug successively can differ by up to a factor of 4.

Gas and liquid permeability measurements were made on 16 samples from Bakken, Eagle Ford, Wilcox and Wolfcamp formations. Higher TOC samples correspond to higher gas to liquid permeability ratios, exacerbating the effect of pore fluid on the permeability measurement.

Contrary to some published literature, permeability creep, i.e. the change of permeability as a function of time at constant net effective stress has been observed to be insignificant. The laboratory measurement time for permeability tests can thus be minimized. This observation also suggests minimal long-term loss of production due to permeability creep. Creep measurements were made on three samples using nitrogen (on a Bakken sample) and dodecane (Wolfcamp samples). With respect to temperature effects, permeability measurements performed at 158 °F on shale samples from Marcellus, Vaca Muerta and Wolfcamp formations indicates insignificant (<10%) change in permeability compared to room temperature measurements. This seems to suggest that permeability

measurements can thus be carried out at room temperature for shale formations, without any significant corrections required for temperature effects.

Two phase flow experiments in shales i.e. flow of oil and gas through water saturated samples reveals the complexity of porous media in shales. Oil (dodecane) showed poor displacement efficiency while flowing through a water saturated Bakken formation sample. NMR results indicate that dodecane does not enter the major connected pore network and is bypassed through alternate flow paths (cracks, fractures etc.). Gas (nitrogen) permeability in a water saturated sample increased with decreasing water saturation. Conducting flow-through experiments with continuous NMR recording can help generate relative permeability curves.

Using MICP (Mercury Injection Capillary Pressure) data, permeability values have been calculated using Kozeny's, Winland's, Swanson's, Kat and Thompson's and Thomeer's methods. These estimates are compared to the corresponding steady-state nitrogen permeability measurements performed on core plugs at an effective pressure of 3000 psi. In some cases, MICP measurements can be performed on drill cuttings and require considerably less time than some permeability measurements.

Nineteen samples from the Bakken, Eagle Ford, Marcellus, Utica, Wilcox and Wolfcamp formations have been used in this study. The MICP derived permeability values using some of the aforementioned methods lie within a factor of 4 of the measured slippage-corrected core plug permeability.

MICP permeability estimates, therefore, can be used as a screening tool to determine the zones of interest over which further analysis can be performed. As MICP measurements can be performed on drill cuttings, high permeability zones can be identified even in the

absence of cores. Selective zonal analysis after the screening proposed by this study can therefore save time and costs significantly.

Chapter 1: Introduction

1.1 Shale Hydrocarbon Resources

Within the U.S., a 92% increase in oil production and almost all growth in the gas production between 2011 and 2014 came from the following shale plays **(Fig. 1)**: Bakken, Eagle Ford, Haynesville, Marcellus, Niobrara, Permian and Utica (EIA, 2017).

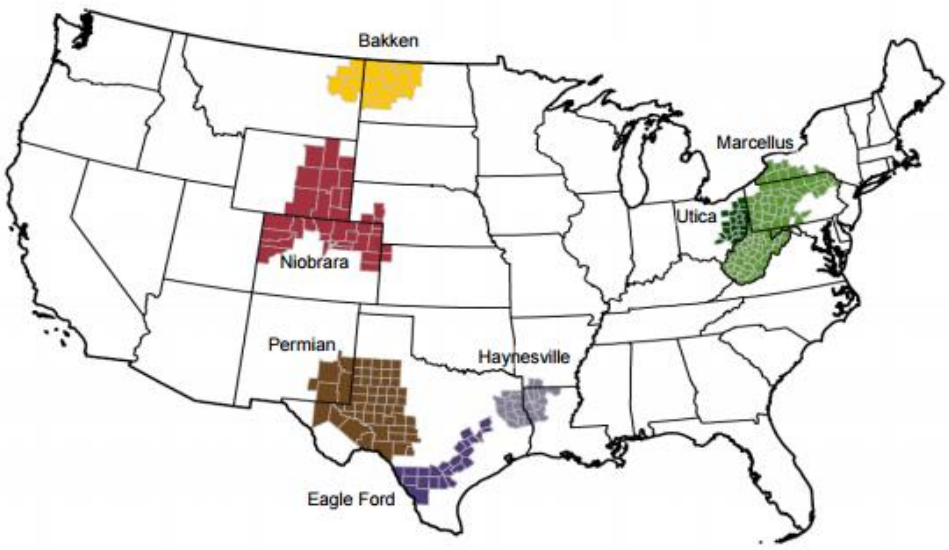

Figure 1: Major US shale plays accounting for 92% oil production growth and all gas production growth between 2011 - 2014 (EIA, 2017).

Low permeability formations will contribute to an increasing percentage in the energy mix, both within the U.S. and shale resource-rich countries all across the world. There is a need to better understand and characterize these formations to optimize production.

1.2 Objective

The objectives of this thesis are to understand

- **Effects of pore fluid, creep and temperature on shale permeability measurements**
  a) Shales have a complex porous structure due to presence of organics as well as inorganics and may not have a pore fluid-independent permeability. Variation in permeability when using different pore fluids (permeants) can be significant. It is important to characterize this difference as these values impact completion design.
  b) If permeability changes significantly as a function of time (creep), it has important implications on the long-term reservoir performance as well as laboratory measurements.
  c) Reservoir temperatures are higher than laboratory room temperature. It is therefore important to understand the dependence of permeability measurements on temperature or the lack thereof.
- **Two phase flow in shales**

  To gain a qualitative understanding of two phase flow in shales by studying displacement in water saturated cores by gas (nitrogen) and oil (dodecane).
- **Estimation of shale permeability using Mercury Injection Capillary Pressure (MICP) data**

  Indirect estimation of permeability using MICP data can serve as a valuable screening tool to determine the zones of interest. This method can also aid in

characterizing permeability in the absence of core, as MICP measurements can be performed on drill cuttings.

Chapter 2: Literature Review

2.1 Matrix Permeability of Shale

Permeability in shales is often several order of magnitudes lower than conventional reservoir rocks and their permeability is often quantified in the nanodarcy range (Wang et al., 2016). This is attributed to small pore sizes in shales (Bustin et al., 2008; Tinni et al., 2012). SEM images taken by Loucks et al., (2009) and Curtis et al. (2010) indicate that pore sizes in shale can be exceedingly small, often just nanometers in diameter. This is further confirmed by NMR measurements (Sondergeld et al., 2010) and BET data (Ross and Bustin, 2009). Presence of organics adds to the complexity of the microstructure by introducing anisotropy and changes in wettability (Curtis et al. 2010; Sondergeld et al., 2010).

Exploiting shale resources involves stimulating the pay zone to enhance its permeability (Morsy et al., 2013). Although fluid flow from hydraulic fractures primarily controls the production performance of a well initially, matrix permeability dictates the ultimate recovery (Heller and Zoback, 2013; Wasaki and Akkutlu, 2015 and Wang et al., 2016). Determination of matrix permeability is thus an important aspect in the overall characterization of a reservoir (Moghadam and Chalaturnyk, 2015). Furthermore, matrix permeability is a key input in reservoir simulation and aids uncertainty reduction in history matching (Sinha et al., 2012 and Heller and Zoback, 2013). It is also required in completion design to optimize fracture spacing. Understanding and quantifying the flow behavior within these low permeability systems, therefore, has direct economic implications which can determine the long-term viability of production.

Laboratory determination of shale permeability is typically done on crushed rock samples or core plugs (Guidry et al., 1996, Luffel et al., 1993). Pressure decay technique on crushed rock was first employed by Luffel et al. (1993) to measure permeability of shales. However, this method has been found to have several inadequacies including lack of repeatability (Passey et al., 2010), dependence of measured permeability on the size of the crushed rock sample, inability to apply a confining stress and lack of directional sensitivity (Cui et al., 2009; Profice et al., 2012; Tinni et al., 2012) .

Plug permeability measurements can be performed by using transient or steady state methods. Transient methods include pressure-pulse decay (Brace et al., 1986; Jones, 1997; Hsieh et al., 1982; Dicker and Smits, 1988) and pressure build up (Metwally and Sondergeld, 2011). Other transient techniques have also been developed by Clarkson et al. (2012) and a 'step decay' technique by Lasseux et al. (2012).

The steady state method is a reliable technique for permeability measurement. It can be accomplished by applying a constant differential pressure across the core plug and computing the steady state (time invariant) flow rate. Darcy's Law can then be used to determine the permeability of a rock with the assumptions of fluid incompressibility, rock fluid non-interaction, rock homogeneity and laminar flow through the core plug. However, the time for such a measurement is generally greater than transient methods (Metwally and Sondergeld, 2011). Furthermore, the pressure differential across the core plug must be kept low to ensure laminar flow.

Permeability measurements from transient techniques (pressure pulse decay and pressure build up) have been found to be comparable, i.e. within 30% of steady state permeability values (Jin et al., 2015; Mathur et al., 2016).

Depending on the measurement conditions and the permeant used, permeability measurements may need to be corrected using appropriate flow regime paradigms. Apparent permeability measured using gas is higher than the intrinsic permeability of porous media due to gas slippage at the pore walls (Klinkenberg, 1941). However, Klinkenberg's correction might not be adequate to estimate permeability of tight formations at low pore pressures. Second order corrections (Beskok and Karniadakis, 1999; Civan, 2010; Sakhaee-Pour and Bryant, 2012; Fathi et al., 2012) can better quantify the flow behavior in low permeability media.

Mathur et al. (2016) characterized the flow regimes in shale and recommended the appropriate slippage correction at different pore pressure levels. At pore pressures of less than 250 psi, transition flow was found to be dominant; double slip corrections are appropriate for this pressure range. For higher pore pressures ≈ 1000 psi, slip flow dominates and Klinkenberg corrections are deemed appropriate for this pressure range. At pressures greater than 2000 psi, the slippage corrections are negligible. Measurements done at these pore pressures can be used without corrections.

In this thesis, all permeability measurements have been carried out using steady state and at a pore pressure of at least 2000 psi.

2.2 Effect of Pore Fluid, Creep and Temperature on Permeability Measurements

2.2.1 Effect of Pore Fluid

Mathur (2015) measured the difference in magnitude of steady state permeability while using dodecane and nitrogen as pore fluids for seven Wolfcamp shale samples (**Fig. 2**). These measurements were carried out at a pore pressure of 3000 psi to avoid any

significant slippage effects and at an effective pressure of 3000 psi. The porosity for these samples varied between 2 - 10%, while the TOC ranged between 0 and 4 wt. %. The reported nitrogen permeability was greater than dodecane permeability by as much as a factor of 2.

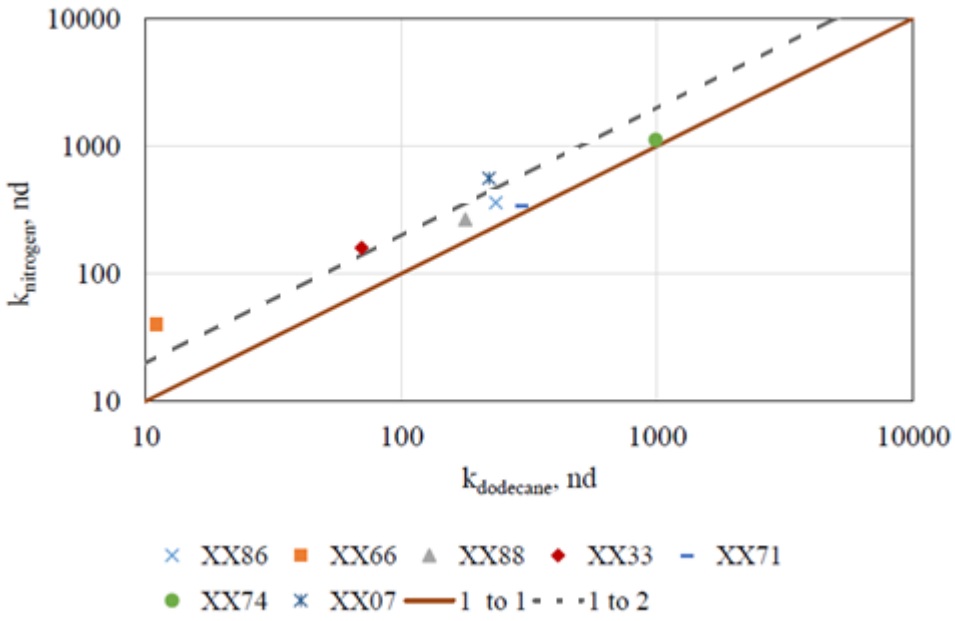

Figure 2: Comparison of nitrogen and dodecane permeability for seven Wolfcamp shale samples (Mathur, 2015). Nitrogen permeability is higher than dodecane permeability by up to a factor of approximately 2.

Brezovski and Cui (2013) and Chhatre et al. (2014) also performed liquid and gas permeability measurements on different shale samples. Brezovski and Cui (2013), performed pulse decay measurements on five Montney shale samples using helium and decane. They found a difference of as high as an order of magnitude between these measurements. Chhatre et al. (2014) performed steady state measurements on eight Vaca Muerta shale samples at reservoir pressure and temperature conditions using both liquid and gas. They found that the slippage corrected gas permeability for some of the samples

was higher than the measured liquid permeability by up to a factor of two. These results indicate that the permeability of nanoporous shales is dependent on the pore fluid.

Matrix drainage in tight gas wells is characterized by transient linear flow regime (Bello, 2009). The distance of investigation (DOI) concept can be used to design the spacing between different stages in hydraulic fracture treatments (Zheng, 2016). Wattenbarger et al. (1998) related the distance of investigation during the linear flow regime to the square root of matrix permeability. Differences in magnitude of permeability even by a factor of up to 4 will have an impact on the number of fracture stages required to drain the reservoir optimally.

The total cost of hydraulic fracture treatment per stage can be as high as $200,000, with average cost per stage in the Bakken field being $125,000 (Oilfield Technology, 2013). The cost per stage of fracture treatment in STACK play in Oklahoma for a 10,000 ft. lateral averaged at approximately $215,900 (OKOGA, 2017).

2.2.2 Effect of Creep

Permeability creep measurements are important to quantify the long-term production performance of a reservoir. Laboratory measurement times can also be affected, if significant creep effects are observed. Long term permeability creep measurements over a period of several weeks have been performed by several authors on Berea sandstone and Horonobe mudstone (Yashura et al., 2012) as well as several shale formations (Chhatre et al., 2014; Mathur, 2016).

Yashura et al. (2012) measured steady state permeability of Berea sandstone using water as the pore fluid over a period of 400 days. The first set of experiments were conducted

at room temperature of 20 °C (68 °F) at two effective stresses of 7.5 and 15 MPa (1100 and 2200 psi). There were no significant changes observed at either effective stress for the first 300 days, wherein the permeability remained around 10 md and 2 md for the lower and higher effective stresses respectively.

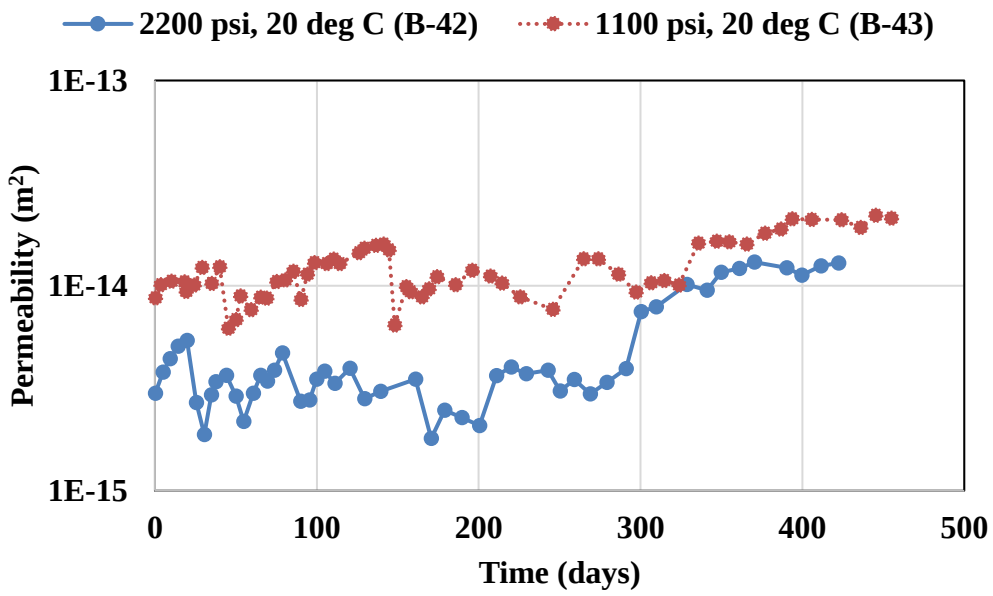

Figure 3: Permeability of two Berea sandstone samples at confining pressure of 1100 psi and 2200 psi over a period of over 400 days measured at 20 °C (68 °F) (Yashura et al., 2012). Change in permeability up till 300 days is minimal.

The permeability increased after 300 days for both samples (**Fig. 3**). The increase in permeability is attributed to mineral dissolution with time. The second set of experiments performed at 90 °C (194 °F) yielded similar results, with the permeability registering an increase at 200 days (**Fig. 4**). A similar pattern is also observed for a fractured Horonobe mudstone sample in their study. At higher temperature, the period of permeability increase was advanced by ~100 days. The dissolution is exacerbated at a higher temperature causing the permeability increase to occur earlier.

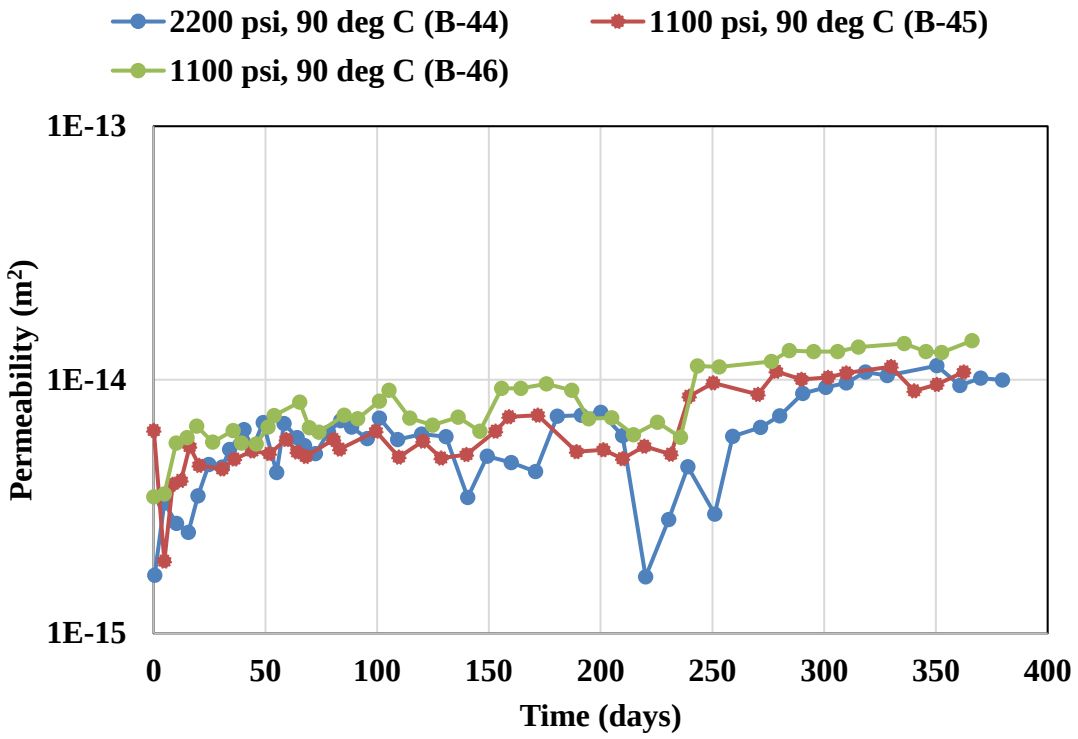

Figure 4: Permeability of three Berea sandstone samples at confining pressure of 1100 psi and 2200 psi over a period of around 400 days measured at 90 ° C (194 °F) (Yashura et al., 2012). The permeability changes are minimal up till 200 days of measurement.

Permeability creep measurements reported by Chhatre et al. (2014) on Vaca Muerta shales at multiple effective stresses indicate a significant change in permeability over a period of eight weeks (**Fig. 5**). The permeability measurements were conducted using steady state method and toluene as the pore fluid. Permeability reduced by around 75% within the first 30 days. They recommend, therefore, to 'stress age' the samples i.e. subject the samples to reservoir pressure conditions for a period of time as long as a month before conducting permeability measurements. Stress aging of a sample to reach a stable value of permeability then becomes particularly important for transient methods of

permeability measurement, wherein the individual experimental duration is typically shorter than that of steady state method.

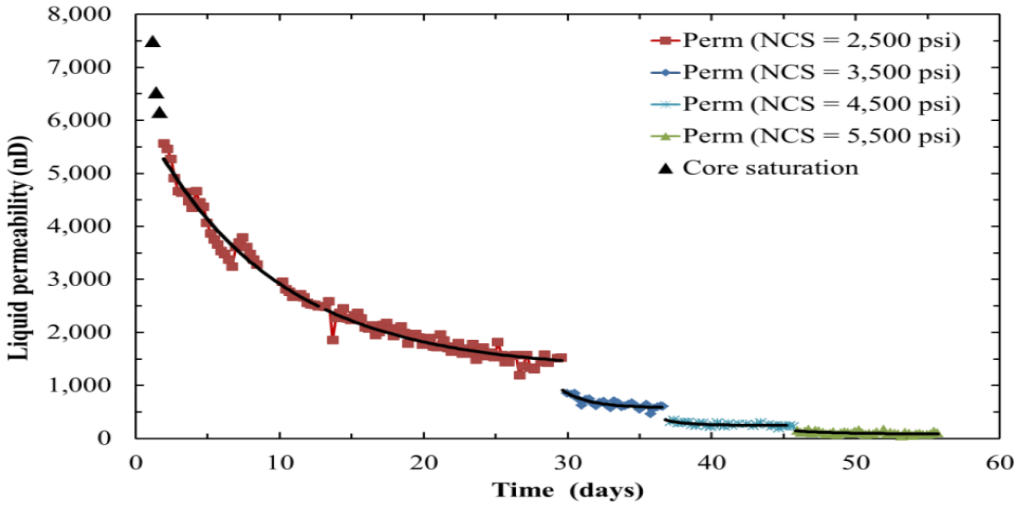

Figure 5: Permeability of a Vaca Muerta shale sample at multiple net confining stresses (2500 – 5500 psi) over a period of eight weeks using toluene\decalin as the pore fluid (Chhatre et al., 2014). Permeability value reduces significantly within the first 30 days of measurement.

However, it must be noted that toluene is an organic solvent. It is not recommended for use as a permeant as it can react with organics within the shale samples. The significant creep observed can possibly be a consequence of the choice of pore fluid used.

Mathur (2015) performed permeability creep measurements on Wolfcamp, Vaca Muerta and Eagle Ford shale. He used liquid (dodecane) and gas (nitrogen) as pore fluids for these tests. Pressure build-up method (transient) was used for Eagle Ford samples. All other measurements were done using steady state method.

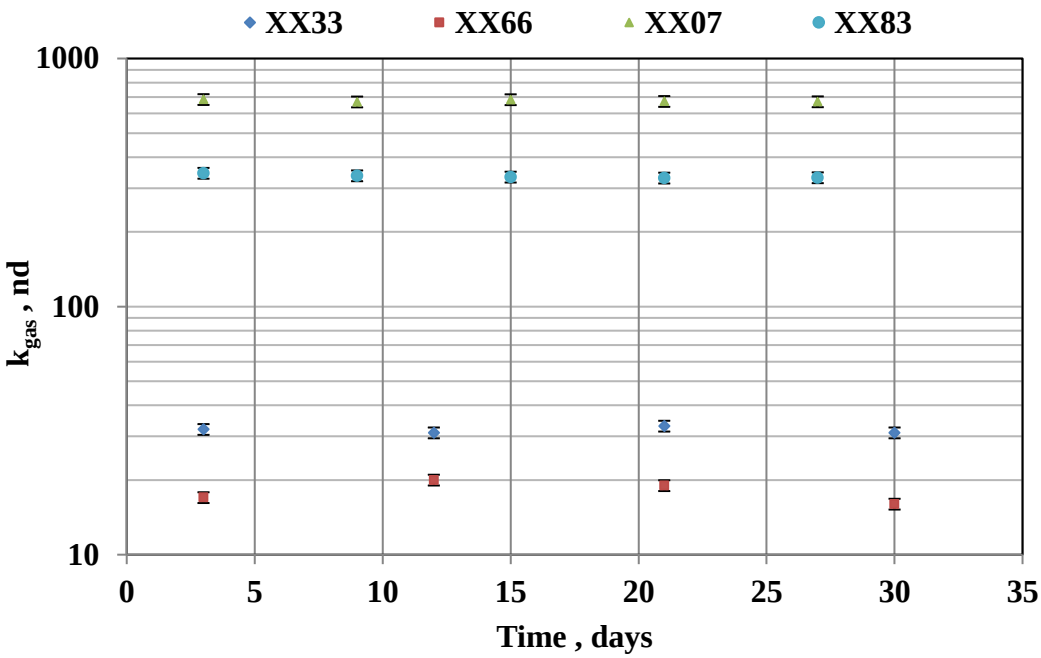

Figure 6: Steady state permeability measurement for four Wolfcamp shale samples over a period of 30 days. Insignificant change in permeability observed (Mathur, 2015).

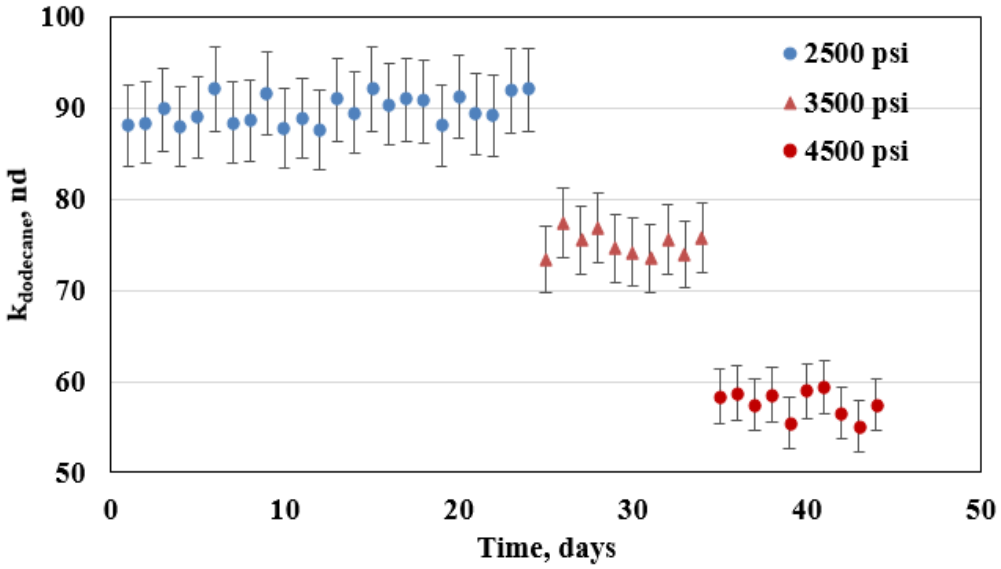

Figure 7: Permeability of a Vaca Muerta shale sample at multiple net confining stresses (2500 – 4500 psi) over a period of six weeks. Insignificant change in permeability observed at each net confining stress (Mathur, 2015).

Permeability creep was insignificant for steady state as well as transient methods. Creep behavior was negligible using either nitrogen or dodecane as the permeant. No creep was observed for Wolfcamp and Vaca Muerta shale (**Fig. 6 and 7**) for the entire period of measurement of over a month. A change in permeability of less than 25% was observed for Eagle Ford shale over the same period of time (**Fig. 8**).

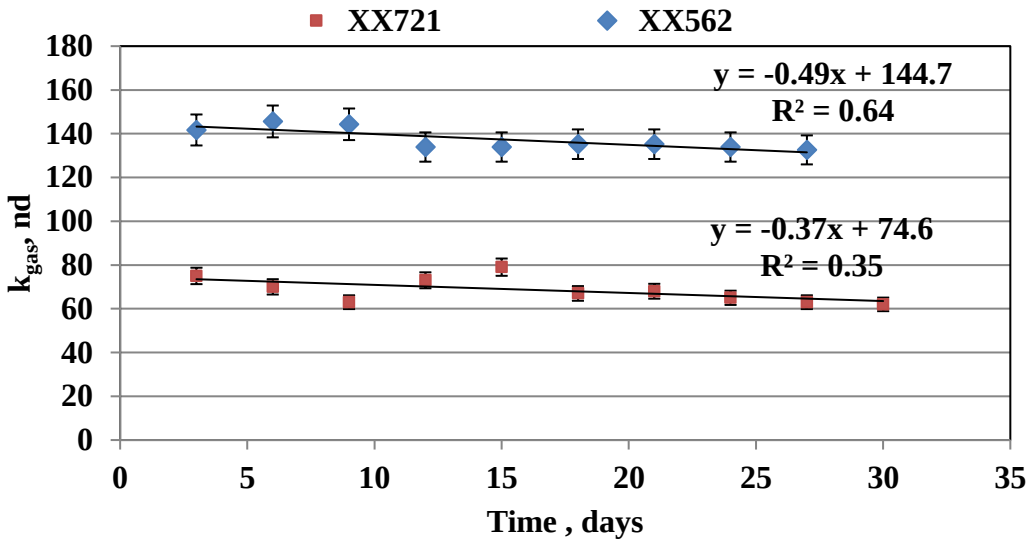

Figure 8: Permeability measurement for two Eagle Ford shale samples over a period of 30 days. Insignificant change (≤ 25%) in permeability observed (Mathur, 2015).

2.2.3 Effect of Temperature

The average reservoir temperatures of a majority of shale plays including Barnett, Bakken, Fayetteville, Horn River, Marcellus, Wolfcamp and Woodford are less than 200 °F, while those for Eagle Ford and Haynesville are higher than 300 °F (Bangia et al., 1993; Roth, 2011).

Sinha et al. (2013) studied the effect of elevated temperature on permeability using steady state permeability measurements for four shale samples at reservoir effective stress and a pore pressure of 125 psi. The measurements were performed using helium at two different

temperatures: 72 °F and 230 °F. They found that the permeability was consistently lower at the higher temperature for all four samples by 3 – 25% (**Fig. 9**). This was attributed to reduction in the size of pore throats due to swelling.

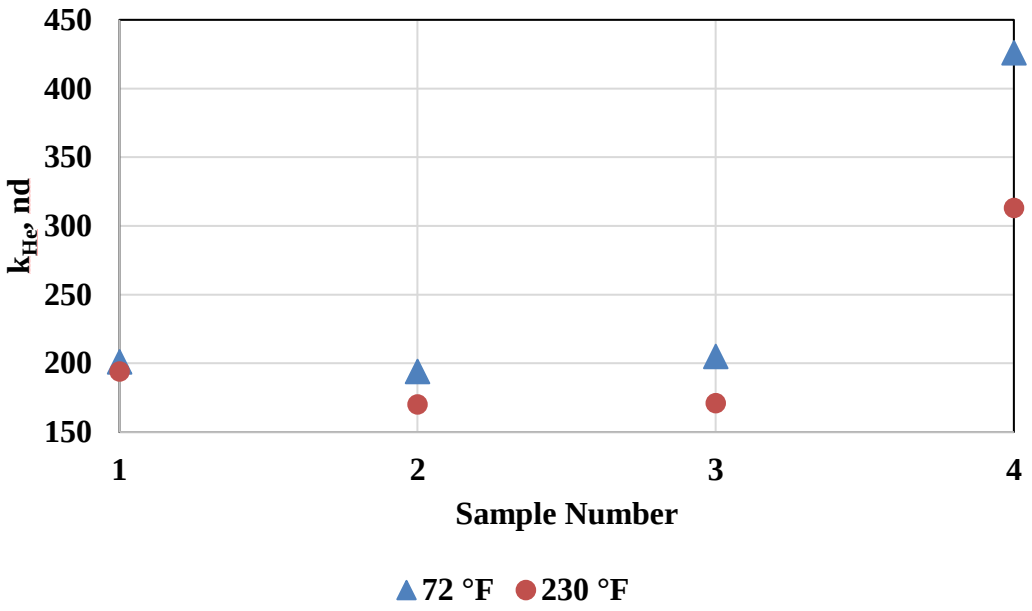

Figure 9: Permeability of four shale samples at 72 °F and 230 °F measured using steady state method. Modified after Sinha et al. (2013).

Such a difference is not significant for ultra-low permeability formations. At low pore pressures (125 psi) gas slippage should be dominant. The reported permeability values are not slippage corrected. The mean free path of gas (λ) is temperature dependent.

$$\lambda = \frac{k_b . T}{\sqrt{2} P . \pi . d_g^2} \quad (1)$$

Where P: Gas pressure, [Pa]

d_g: Effective diameter of a gas molecule, [m]

k_b: Boltzmann constant, [1.3807×10^{-23} J/K]

T: Temperature of the gas, [K]

R: Gas constant, [8.314472 J/(K.mol)]

N_A: Avogadro number

According to **Equation 1**, mean free path should be greater at elevated temperature. Lower permeability at higher temperature is therefore unexpected.

Yashura et al. (2012) studied the long-term evolution of permeability for Berea sandstone at room temperature (68 °F) as well as at an elevated temperature (194 °F). The onset of permeability increase was advanced by ~100 days at the higher temperature. This change in trend is attributed to mineral dissolution over a period of time, which was more pronounced at elevated temperatures (**Fig. 3 and 4**).

The effect of temperature on permeability evolution is relevant for in-situ oil shale extraction. Yang et al. (2012) quantified the permeability evolution with increasing temperature for Daqing and Changqing oil shales. They used nitrogen as the permeant for steady state measurements over a temperature interval of 200 °C to 500 °C (392 °F – 932 °F). The authors reported a critical temperature for both the samples below which a reduction in permeability was observed with increasing temperature. With further increase in temperature, the permeability increased as well (**Fig. 10**).

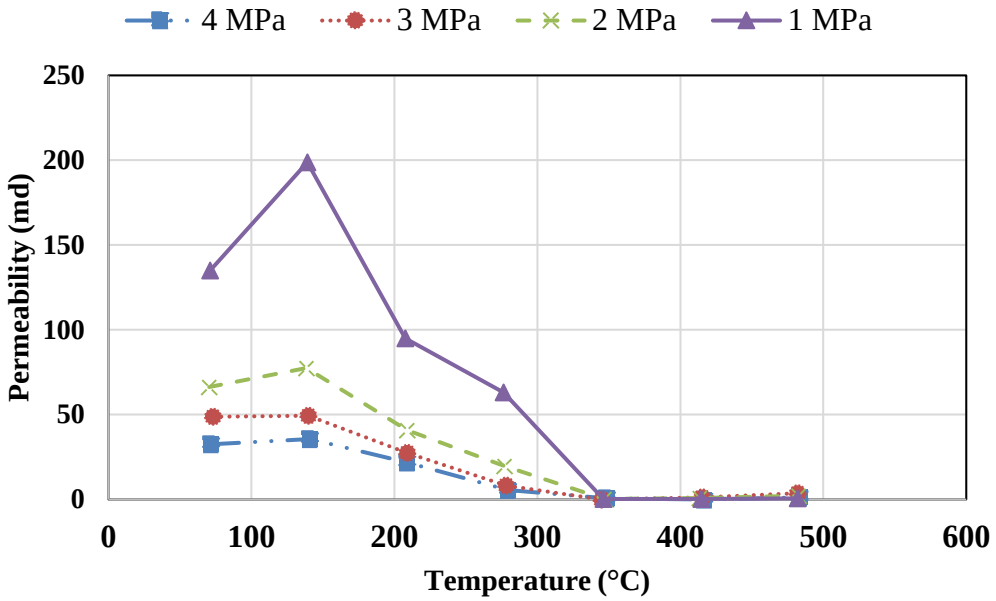

Figure 10: Evolution of permeability in Daqing oil shale with increasing temperature at different pore pressures. Nitrogen was used as the permeant at pore pressures ranging from 1 to 4 MPa. Permeability decreases up till the critical temperature of ~350°C is achieved and increases thereafter. (Yang et al., 2012).

2.3 Two Phase Flow in Shales

Complexity of fluid flow mechanisms and wettability in shales is affected by its lithology, pore structure and presence of organics (Lan et al., 2014). Shale pores generally tend to have mixed wettability due to presence of both organics and inorganics (Odusina et al., 2011).

NMR measurements before and after permeability measurement using nitrogen as well as dodecane on a Wolfcamp shale core plug by Mathur (2015) showed that water saturation within the sample remained unchanged (~22%). The helium porosity of the sample was 7.2%, while the TOC was 1.2 wt.%. Permeability measurements in shales are essentially relative permeability measurements.

NMR response of brine and oil imbibition on Barnett, Haynesville and Woodford shale core plugs suggest that brine saturated porosity is higher than the oil saturated porosity (Tinni et al., 2014). Furthermore, the NMR responses show that oil and methane have access to a limited fraction of pore spaces, while brine is able to access the entire pore spectrum. Flow path in the shales studied is controlled primarily by the water-wet porosity.

2.4 Permeability Estimation from MICP Data

Mercury injection capillary pressure, MICP, data for rock samples can be used to estimate permeability. Purcell (1949) first demonstrated that permeability could be derived from capillary pressure curves generated by injecting mercury into porous media. By combining Poiseuille's equation with Darcy's Law for a bundle of tubes and introducing a lithology factor 'F' to account for the intrinsic properties of fluid flow media, he proposed an equation to estimate permeability:

$$\mathbf{k = 2F(\sigma cos\theta)^2 \int_0^1 \frac{dS_{nw}}{dP_c^{\,2}}} \qquad \textbf{(2)}$$

Where:

k: Permeability, md

F: Lithology factor

σ: Interfacial tension, dynes/cm

θ: Contact angle, degrees

P_c: Capillary pressure, psi

S_{nw}: Non-wetting phase saturation, fraction

Over the years, several other empirical models have been developed. Comisky et al. (2007) applied thirteen different empirical models to estimate the permeability of 63 tight gas sand rock samples from five different basins across Argentina and the United States. In their study, the Klinkenberg corrected steady state permeability for the samples ranged from 0.0001 md – 0.20 md, while the porosity varied between 2 – 15%. They found that the estimates of permeability from the empirical models considered were inaccurate for these tight gas sand samples (with permeability in all cases lower than 0.20 md). Their measured permeability values cross plotted against Winland correlation (Pittman, 1992) are shown in **Fig. 11** and **Fig. 12**. As can be seen, both correlations overestimate the permeability for most samples.

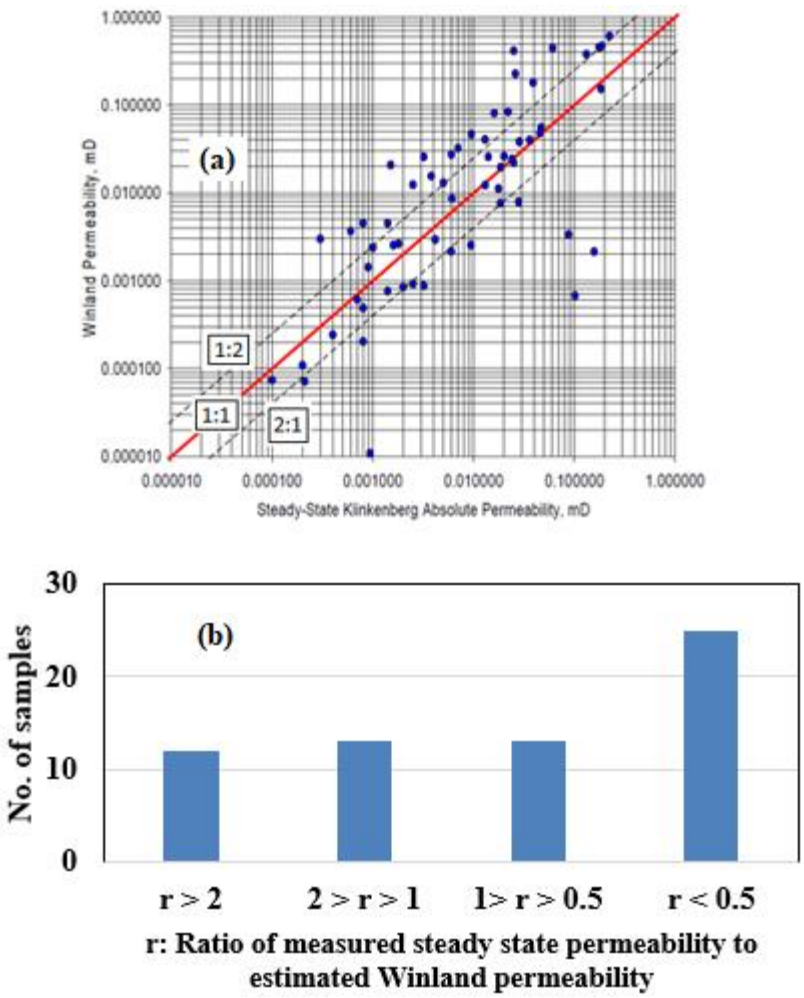

Figure 11: (a) Crossplot showing the measured permeability (Klinkenberg corrected steady state) against the estimated permeability from Winland correlation (Comisky et al., 2007). (b) Histogram depicting the data in four discrete sets with varying ratio 'r' i.e. the ratio of Klinkenberg corrected steady state to estimated Winland permeability.

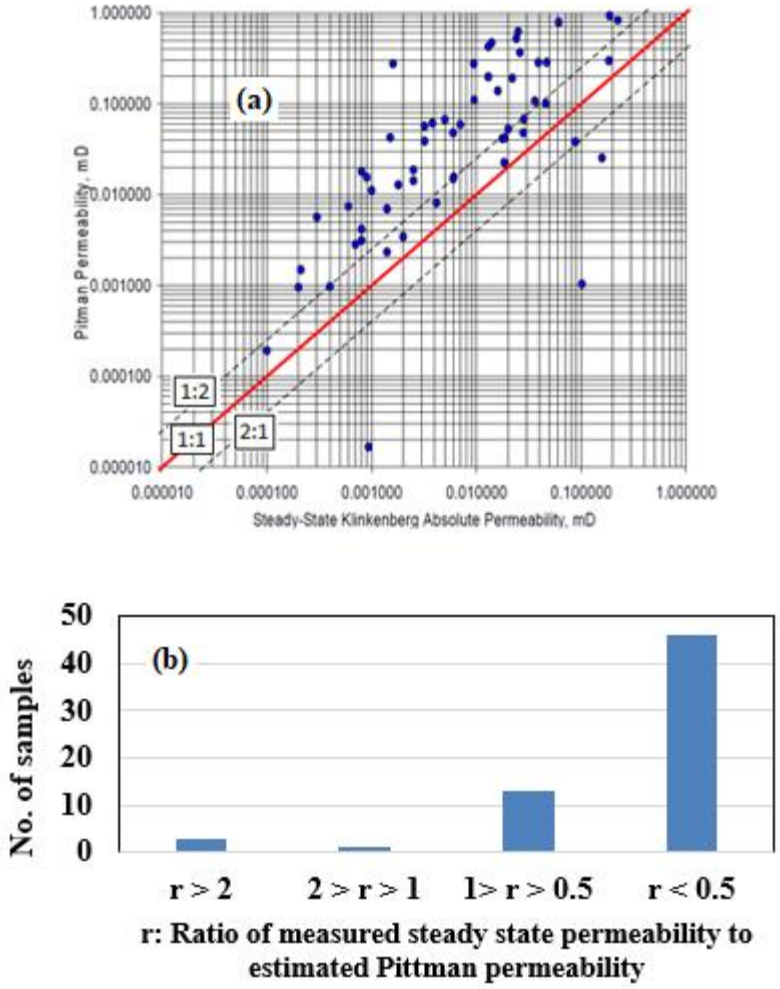

Figure 12: (a) Crossplot showing the measured permeability (Klinkenberg corrected steady state) against the estimated permeability from Pittman correlation (Comisky et al., 2007). (b) Histogram depicting the data in four discrete sets with varying ratio 'r' i.e. the ratio of Klinkenberg corrected steady state to estimated Pittman permeability.

Chapter 3: Experimental Methodology

Permeability measurements on core plugs reported in this thesis have been performed using the steady state method described earlier. This chapter details the experimental setup used for making these measurements and the underlying procedure to calculate permeability.

3.1 Steady State Method

Steady state method to measure permeability involves maintaining a constant pressure differential between the upstream and downstream side of a core sample and measuring the flow rate of the pore fluid (permeant) through it as a function of time. When steady state is achieved, i.e. a constant flow rate, permeability is measured using Darcy's Law. According to Darcy's Law, flow rate of an incompressible fluid through a homogenous porous medium under laminar flow condition with no interaction between the fluid and the medium is given by

$$\mathbf{k = \frac{q\mu L}{A\Delta P}} \qquad \textbf{(3)}$$

Where:

k: Permeability (Darcy)

q: Flow rate (cm^3/s)

A: Cross-sectional area (cm^2)

ΔP: Pressure difference across the sample (atm)

μ: Viscosity of the permeant (cP)

L: Length of the sample (cm)

For the above equation following assumptions are made: (a) pore fluid is incompressible, (b) the porous medium is homogenous (c) the fluid flow through the medium is in the laminar flow regime, and (d) there is no rock-fluid interaction.

Typically, steady state permeability measurements are made using gas, i.e. nitrogen or helium, which are compressible. The behavior of these gasses at different pressures can be described using Boyle's Law. At constant temperature:

$$\mathbf{P_1V_1 = P_2V_2} \quad \textbf{(4)}$$

Where:

P_1, P_2: Pressure of the gas upstream and downstream

V_1, V_2: Volume of the gas upstream and downstream

For steady state flow across a constant cross sectional area,

$$\mathbf{P_1q_1 = P_2q_2 = P_mq_m} \quad \textbf{(5)}$$

Where:

P_m, q_m: Pressure and flow rate of the gas at mean pore pressure

The mean pore pressure is calculated as the simple average of the upstream and downstream pressure at two ends of the test core plug.

$$\mathbf{P_m = \frac{P_1 + P_2}{2}} \quad \textbf{(6)}$$

Accounting for the compressibility of gas, permeability value can thus be calculated at the mean pore pressure using either the upstream (P_1, V_1) or the downstream (P_2, V_2) parameters using Darcy's Law (**Equation 7**).

$$\mathbf{k = \frac{2\mu Lq_1P_1Z_m}{A(P_1^2 - P_2^2)Z_1}} \quad \textbf{(7)}$$

Where:

Z_m: Compressibility factor of gas at mean pore pressure

Z_1: Compressibility factor of gas at upstream pressure

The time taken for steady state permeability measurements is typically greater than transient methods. For low permeability rocks such as shales, flow rates can be in the order of 10^{-5} cm^3/s. Depending on the length of the sample and its inherent permeability, the time taken for flow-through of at least two pore volumes through a core plug sample can be several days. The differential pressure between upstream and downstream is kept small (typically 100 psi) to prevent turbulence in the fluid flow. Reynold's number for fluid flow through a sample core plug of 1.5" length and 1" diameter at typical test conditions (i.e. 2000 psi pore pressure and 76° F) is within the range for laminar flow.

The data collected for permeability calculation for an Eagle Ford shale sample is shown in **Figure 13**.

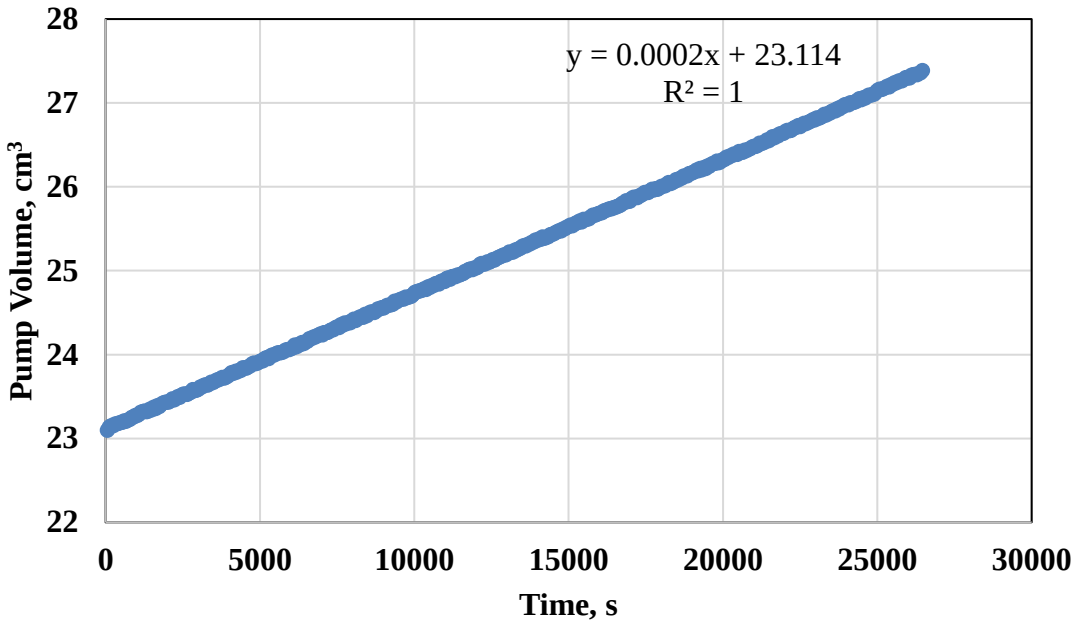

Figure 13: Downstream pump volume as a function of time for permeability measurement of Eagle Ford sample XX149 using nitrogen. The effective pressure is held at 3000 psi. The calculated permeability is 356 ± 18 nd.

In this example, the core sample is subject to a confining pressure of 5000 psi and a mean pore pressure of 2000 psi. The effective pressure on the sample is thus 3000 psi. The downstream pump volume recorded as a function of time is used to calculate the flow rate of nitrogen. This flow rate is used to calculate the permeability of the sample using **Equation 7**. The calculated permeability using nitrogen is 356 ± 18 nd.

3.2 Experimental Setup

A schematic of the experimental setup used for permeability measurements is shown in **Figure 14**. The setup consists of a Hassler type core holder placed inside an oven to minimize temperature variation during measurement. The core sample is held inside a Viton sleeve within the core holder. The confining pressure and pore pressure on the

sample are applied using three individual syringe pumps. Nine pneumatically controlled valves are used to direct fluid flow and maintain pressure. All three pumps and valve actuation are computer controlled. The syringe pumps have a capacity of 103 cm^3. The pressure accuracy over the operational pressure range (0 – 10,000 psi) is 0.5% and the flow accuracy is 10^{-5} ml/min (accurate to 0.3% of the set point).

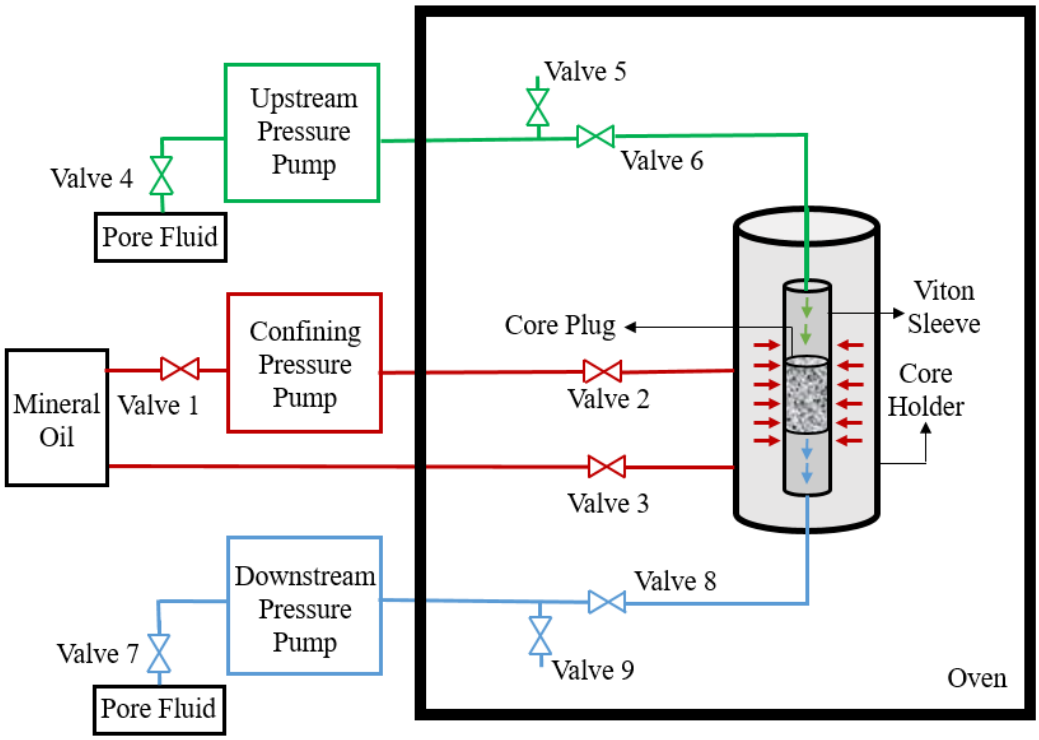

Figure 14: Schematic of the experimental setup used for measuring permeability.

The core holder can accommodate a polished one-inch diameter cylindrical core plug with length varying between 1 to 1.5 inches. The confining pressure pump applies stress radially on the sample surrounded by the Viton sleeve using mineral oil as the confining fluid. The upstream and downstream pumps apply the pore pressure using either gas or liquid.

The system is similar to the permeability measurement setup used by Mathur (2015). Mathur et al. (2016) established that pulse decay and pressure build-up permeability values after appropriate corrections lie within 30% of the steady state permeability values. Steady state permeability measurements provide a standardized method of measuring permeability. Furthermore, reduced number of connection and valves reduce the possibility of pressure leaks. In this thesis, all permeability measurements have been performed using steady state method.

For permeability measurements at elevated temperatures (section 4.1.3), the source (upstream section), sink (downstream section) and the test cell are heated using a silicon heat tape. For temperature control to within ±2 °C of the set point, a J-type thermocouple is used with a controller. Permeability measurement is performed when temperature stabilizes.

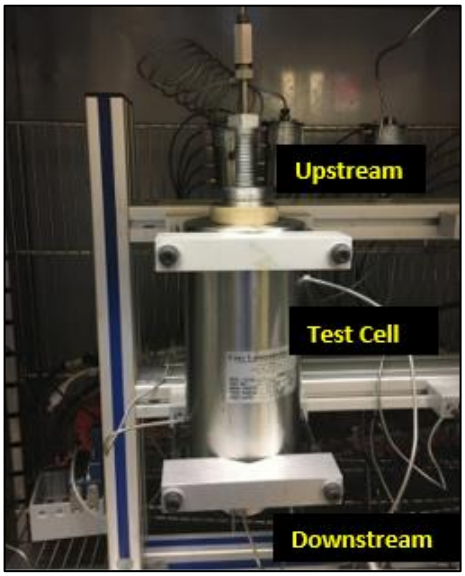

Figure 15: Test cell for permeability measurement. The system consists of an adjustable top end and a fixed bottom assembly. The sample is held inside the core holder within a rubber sleeve.

The core plug sample placed inside the core holder is held between a fixed bottom assembly and an adjustable top end (**Fig. 15**). During heating of the sample, the top assembly is not tightened completely in order to provide room for thermal expansion of the core plug sample, howsoever insignificant. This decreases the possibility of stress cracking by thermal expansion.

Section 4.2 discusses experiments related to two phase flow in shales. To determine the sweep efficiency of dodecane through a water saturated sample, dodecane was flowed through it in the permeability test cell and NMR T_2 spectrum was recorded at different times to calculate the changes in saturation within the sample during the flow experiment. To record the change in saturation with flow of dodecane using NMR, a 'silent' background was required that could be used to saturate the sample prior to flowing dodecane. Heavy water, expected to have an insignificant signal on the NMR T_2 spectrum was chosen. The NMR T_2 spectrum of water and dodecane mixtures was recorded to establish the applicability of heavy water for two phase flow experiments.

NMR T_2 spectrum of heavy water (D_2O) was measured and compared with water (H_2O) and dodecane. 1 cm^3 of water was put in a glass vial with total volume of 7.5 cm^3 and its T_2 spectrum was recorded (**Fig. 16 (a)**). T_2 spectrum of heavy water was recorded in a similar glass vial with total volume 7.5 cm^3 (**Fig. 16 (b)**). Thereafter, 1 cm^3 of water was added to the glass vial containing heavy water and its T_2 spectrum was recorded as well (**Fig. 16 (c)**).

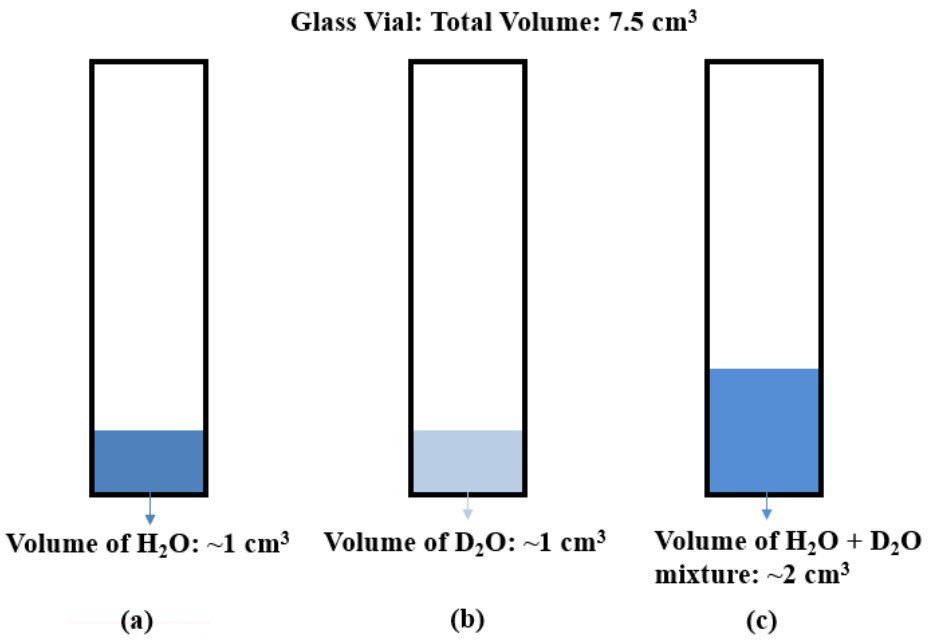

Figure 16: Sample for confirmation of NMR signal for heavy water (D_2O) in the presence of water.

In **Fig. 17**, the volume fraction occupied by liquid is indicated by the cumulative porosity on the NMR T_2 spectrum. 1 cm^3 of heavy water occupies a negligible volume fraction.

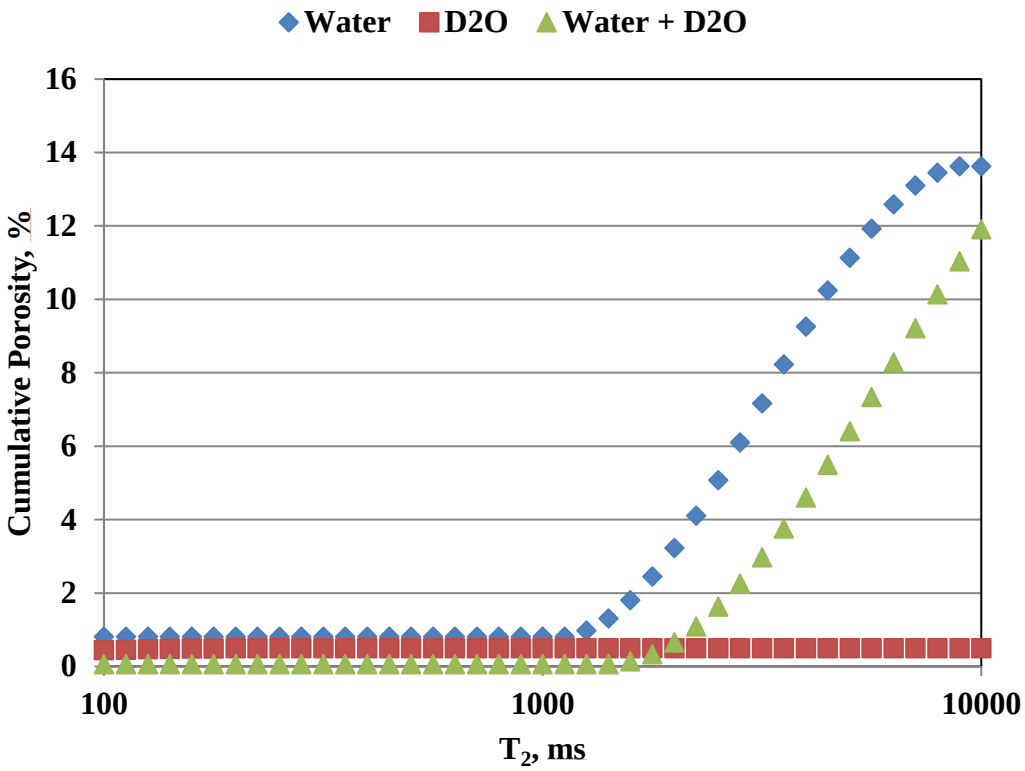

Figure 17: The NMR T_2 cumulative porosity plot for determining the NMR signal for heavy water. The addition of 1 cm^3 heavy water (D_2O) to 1 cm^3 water (H_2O) in the test vial does not alter the cumulative porosity recorded.

Similar measurements were done using dodecane and a mixture of dodecane and heavy water (**Fig. 18**). 1 cm^3 of dodecane was put in a glass vial (**Fig. 18 (a)**). The recorded cumulative porosity on the T_2 spectrum i.e. occupied volume fraction of the glass vial by dodecane is ~15%. Addition of 1 cm^3 of heavy water to the glass vial does not lead to any significant change in the recorded signal (**Fig. 18 (b)**). The NMR T_2 cumulative porosity for these fluids is shown in **Fig. 19**.

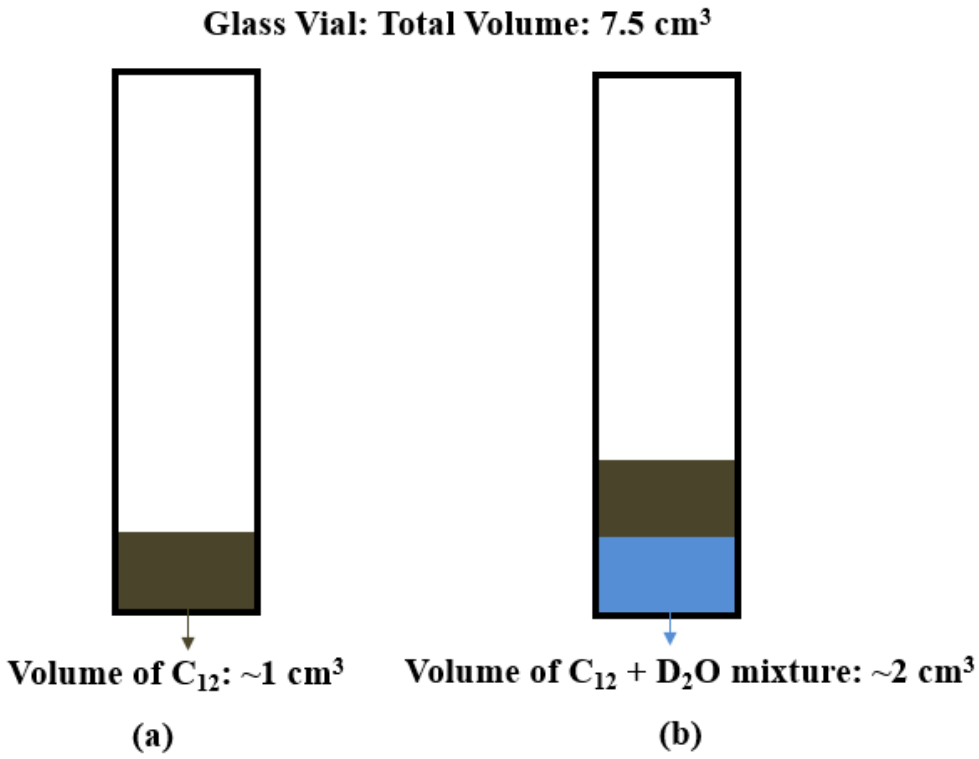

Figure 18: Samples for confirmation of NMR signal for heavy water (D_2O) in the presence of dodecane.

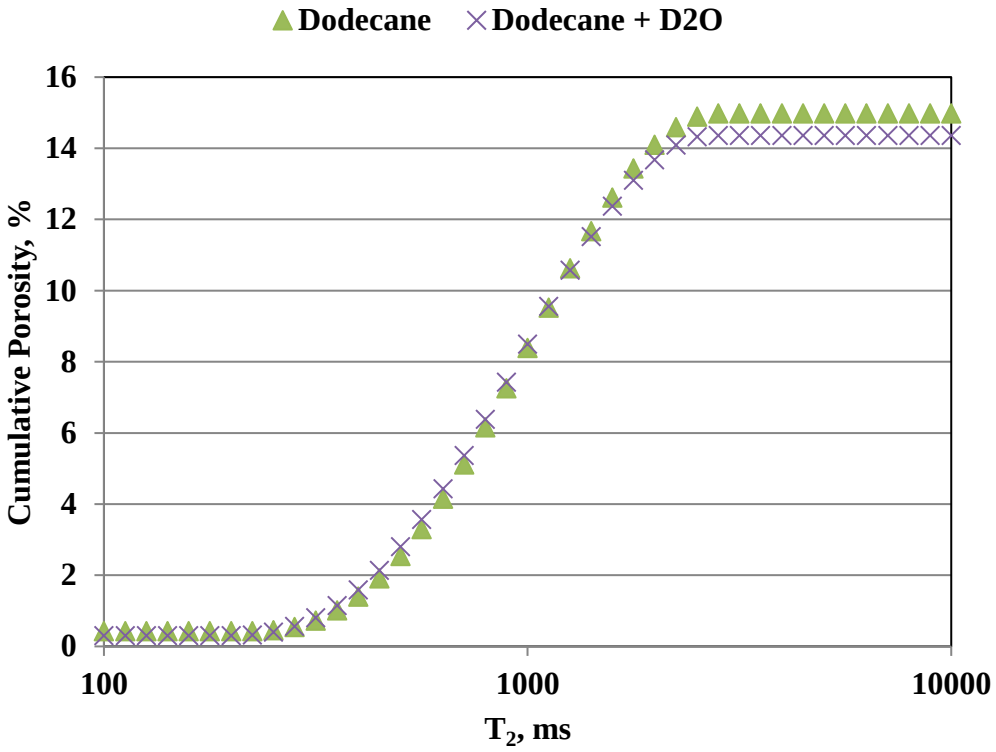

Figure 19: The NMR T_2 cumulative porosity plot for determining the NMR signal for heavy water. The addition of heavy water (D_2O) to dodecane in the test vial does not alter the cumulative porosity recorded.

Heavy water can thus be used as a 'silent' background to record the saturation of water as well as dodecane.

Chapter 4: Results and Discussion

4.1 Effect of Pore Fluid, Creep and Temperature

This section deals with experimental parameters of permeability measurements such as the choice of pore fluid, the length of time over which the measurement is carried out and the temperature maintained during the course of the measurement.

4.1.1 Effect of Pore Fluid

The effect of pore fluid on permeability measurements has been studied using different pore fluids including nitrogen and dodecane on samples from multiple shale formations. The comparison between gas and liquid permeability was performed on a total of 16 samples from Bakken, Eagle Ford, Wilcox and Wolfcamp formations. For the samples studied, helium porosity ranged between 1 and 9%, and the TOC between 1 and 6 wt. %. All measurements were performed at a pore pressure of 2000 psi and an effective pressure of 3000 psi. The difference between upstream and downstream pressures (ΔP) was maintained at 100 psi. **Table 1** shows the FTIR mineralogy for samples from each formation.

Table 1: FTIR Mineralogy, TOC and maturity window for samples used in comparison of liquid and gas permeability

Formation	Sample	Quartz	Carbon-ates	Clays	Feldspar	Other	TOC	Maturity Window
	ID	wt.%						
Wolfcamp	XX40	22	6	62	6	4	2.0	Oil
Wolfcamp	XX12	11	15	60	10	4	1.7	Oil

Wolfcamp	XX48	6	16	56	17	4	2.0	Oil
Eagle Ford	XX937	4	43	44	8	1	3.4	Dry Gas
Eagle Ford	XX063	7	33	49	11	0	3	Dry Gas
Eagle Ford	XX134	1	62	30	4	3	3.9	Dry Gas
Eagle Ford	XX439	0	90	2	4	4	2.7	Conden-sate
Eagle Ford	XX536	0	91	5	0	4	1.0	Conden-sate
Eagle Ford	XX747	0	88	9	1	2	1.7	Conden-sate
Eagle Ford	XX752	3	58	26	7	6	1.7	Conden-sate
Eagle Ford	XX110	3	87	4	2	4	2.5	Conden-sate
Eagle Ford	XX149	3	80	12	2	3	2.5	Conden-sate
Eagle Ford	XX899	2	66	27	4	1	5.7	Dry Gas
Wilcox	XXSH	37	10	43	9	1	1.2	-

(Middle) Bakken	XX90	0	85	8	6	1	2.4	Oil
(Middle) Bakken	XX485	36	33	18	13	0	1.5	Oil

Nitrogen permeability was found to be greater than the dodecane permeability for all samples. As the measurements were performed at pore pressure of 2000 psi, the slippage corrections are negligible. For a majority of the samples (12 out of 15), the difference in magnitude ranged between a factor of 2 to 4. For the other three samples, the difference in magnitude was less than a factor of 2. For a single Eagle Ford sample, the difference in magnitude was found to be a factor of ~8 (**Fig. 20**).

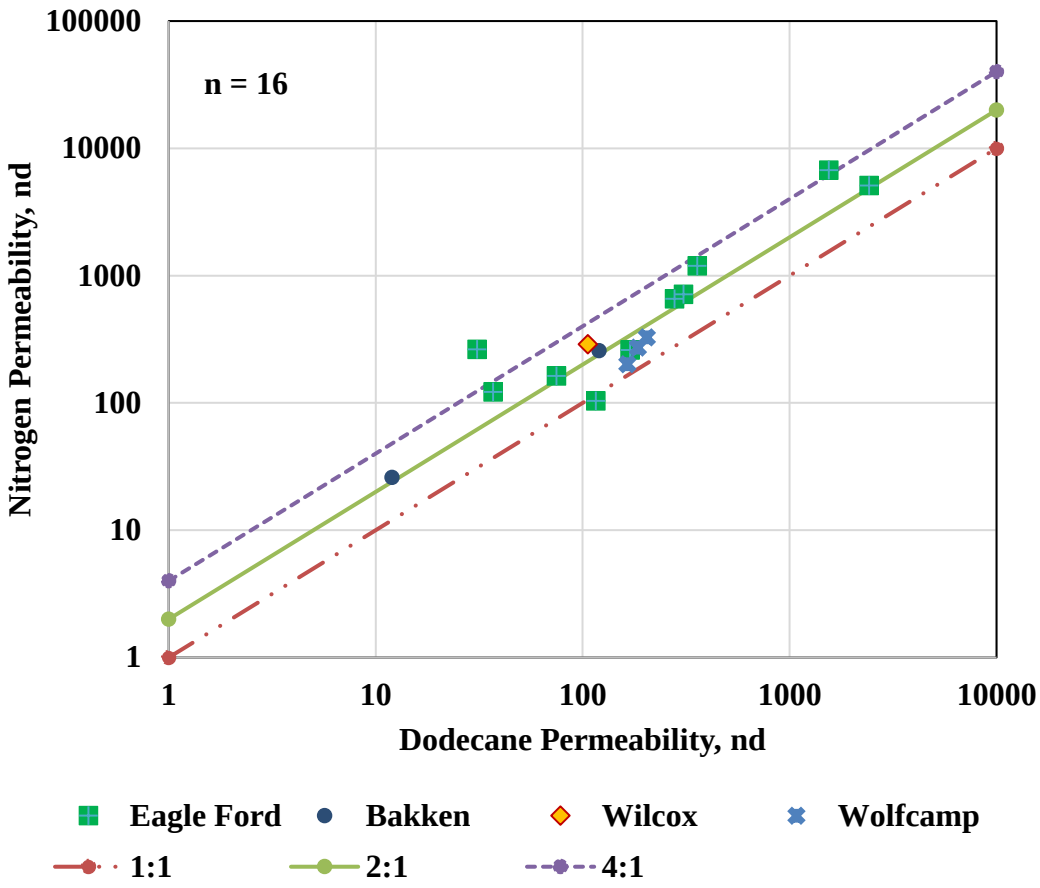

Figure 20: A comparison between nitrogen and dodecane permeability for 16 samples from multiple formations (Bakken, Eagle Ford, Wilcox and Wolfcamp). Nitrogen permeability is higher than dodecane permeability by up to a factor of 4.

As described earlier in Chapter 2, Brezovski and Cui (2013), Chhatre et al., (2014) and Mathur (2015) have also reported differences between the measured liquid and gas permeability, ranging between a factor of 2 to well over an order of magnitude.

Nitrogen to dodecane permeability ratio for the three Wolfcamp samples studied lies between 2.2 to 2.7. These samples have similar helium porosities (6.5 – 7.5 %), TOC (2 – 4 wt. %) and clay content (~60%). Mathur (2015) performed measurements on seven Wolfcamp samples using a similar setup. Nitrogen and dodecane were used as pore fluids at an effective stress of 3000 psi. Pore pressure for all measurements was 3000 psi and

ΔP was maintained at 100 psi. Permeability measured on Wolfcamp samples along with Wolfcamp core plug measurements performed by Mathur (2015) using a steady state method as well is shown in **Fig. 21**. For a majority of samples, the gas to liquid permeability ratio is ranges between 1 and 4. Brezovski and Cui (2013) measured the permeability of five Montney shale samples using helium and decane and suggested a power law dependence between liquid and gas permeability.

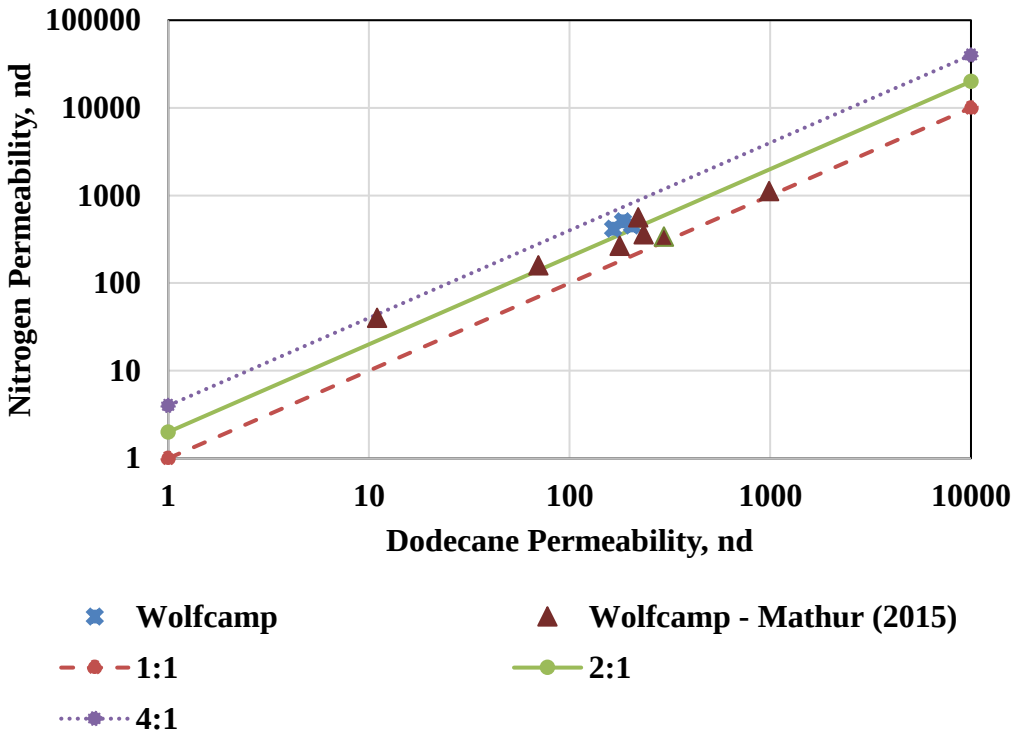

Figure 21: A comparison between nitrogen and dodecane permeability for Wolfcamp shale samples including measurements made by Mathur (2015). Gas/liquid permeability ratios lie between 1 and 4.

Dependence of difference in magnitude between gas and liquid permeability was analyzed as a function of porosity, TOC and clay content for 16 samples (**Figs. 22 (a),**

(b) and (c)). A single Eagle Ford sample with gas permeability approximately eight times higher than its liquid permeability was not included.

The presence of organics and inorganics including clay leads to mixed wettability in shales. NMR measurements performed on a Wolfcamp core plug by Mathur (2015) before and after flowing dodecane indicate that water saturation within the sample remains unchanged. It is possible that oil wet pores could be contributing to a decrease in liquid (dodecane) permeability. Higher TOC should thus correlate with relatively lower dodecane permeability compared to the nitrogen (non-wetting) permeability. **Fig. 22 (b)** shows a weak correlation wherein an increase in the ratio of nitrogen to dodecane permeability corresponds to increasing TOC.

No relation is observed between either porosity or clay content with increasing difference in magnitude of nitrogen to dodecane permeability (**Figs. 22 (a) and (c)**).

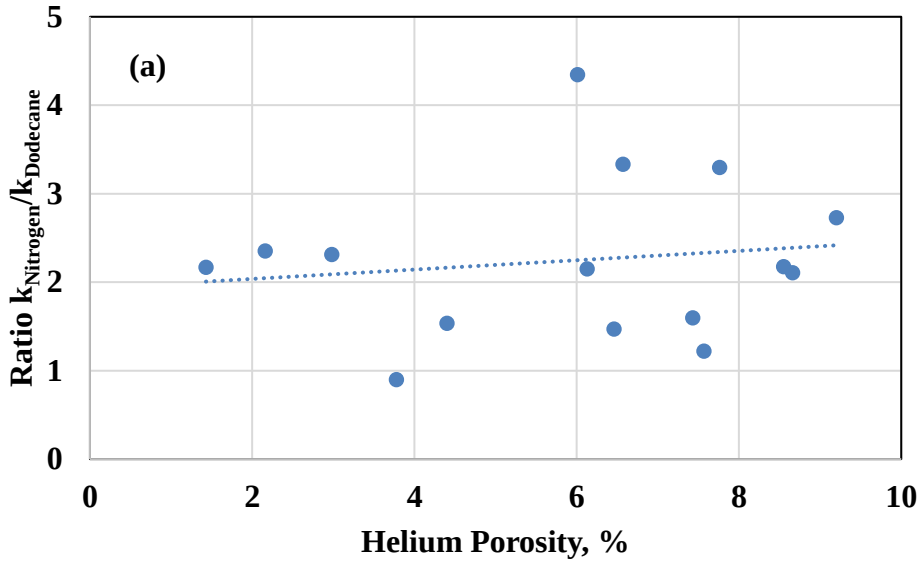

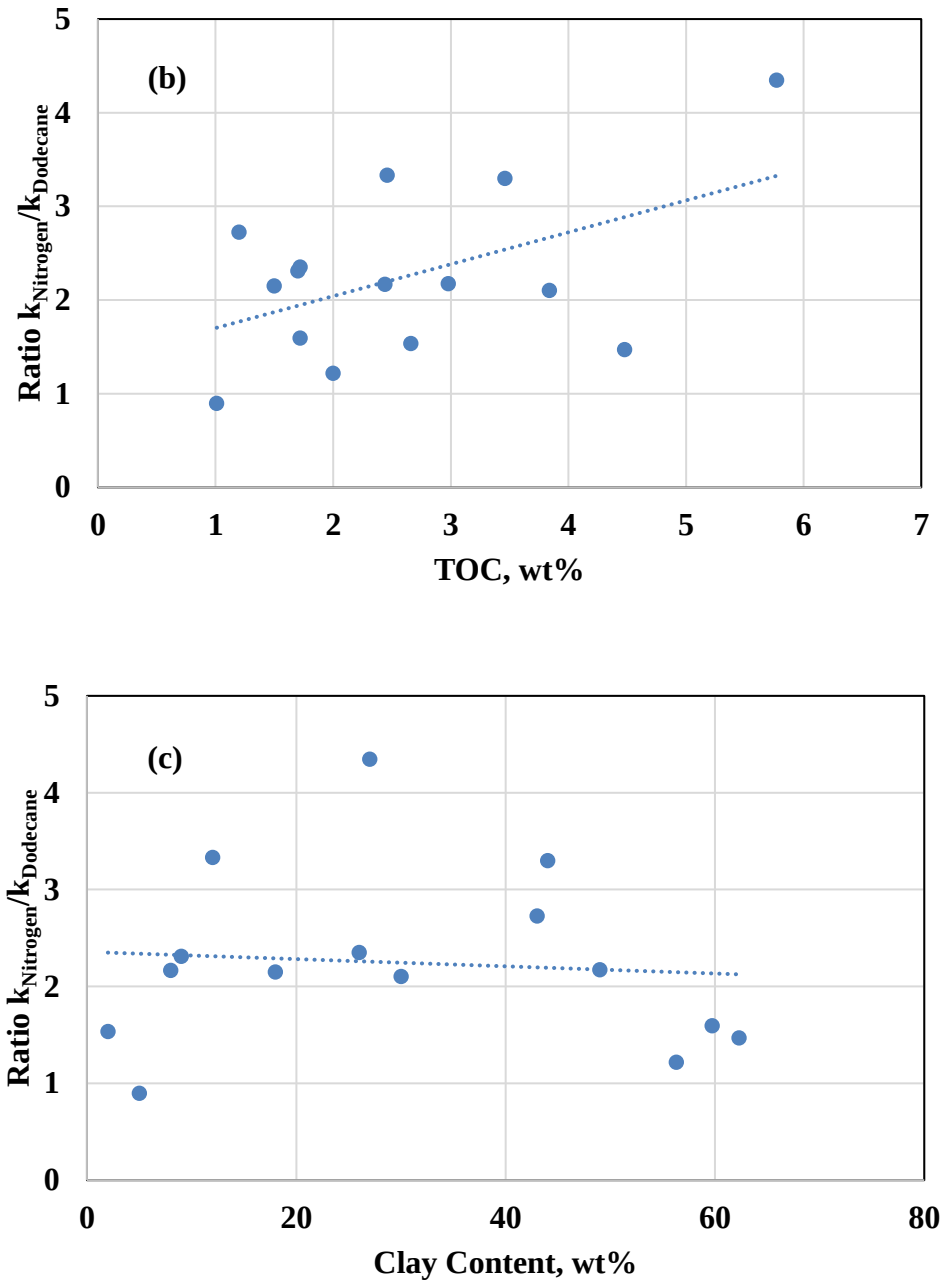

Figure 22: Ratio of nitrogen permeability to dodecane permeability for 15 shale samples sample plotted against (a) helium porosity, (b) TOC and (c) clay content. Nitrogen to dodecane permeability ratio increases with increasing TOC. Porosity and clay content do not show any correlation with the gas to liquid permeability ratio.

Gas permeability values for a majority of samples have been found to be up to four times higher than the corresponding liquid permeability. Gas/liquid permeability ratio of up to 4 can lead to an overestimation in the distance between fracture stages by a factor of 2. Using gas permeability to characterize oil or condensate systems for designing fracture treatments can thus double the estimated distance between fracture stages. Optimum drainage of a play may thus require greater number of fracture stages than estimated using gas permeability.

The total cost of hydraulic fracture treatment can vary significantly across different plays and operators, as well as wellbore specifics. Assuming an average cost of $150,000 per fracture stage, the total cost of well completion can vary significantly based on number of fracture stages. The correct estimation of permeability can thus help reduce costs of well completion.

4.1.2 Effect of Creep

Permeability creep measurements entail applying a constant net effective stress, i.e. constant pore pressure and confining pressure to a sample, and recording the evolution of permeability with time.

Creep measurements were performed on one Bakken sample (Upper Three Forks) using nitrogen as pore fluid and two Wolfcamp samples using dodecane.

The FTIR mineralogy for the Bakken (Upper Three Forks) sample from the oil window is shown in **Fig. 23**.

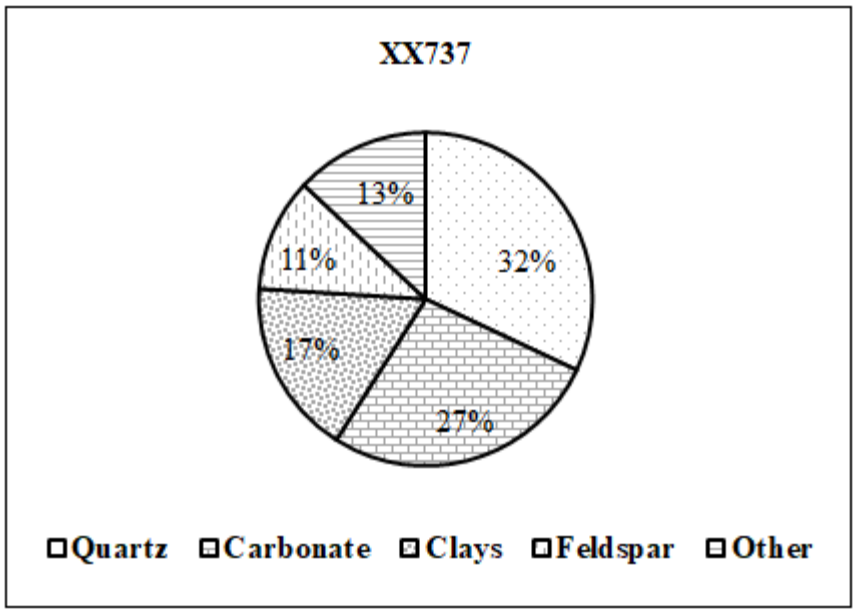

Figure 23: FTIR mineralogy for sample XXX37 (Bakken – Upper Three Forks).

The helium porosity of the sample is 6%. The permeability of the sample was recorded for a period of 10 days with a measurement performed every 24 hours. The pore pressure was kept at 2000 psi, and the effective pressure was maintained at 3000 psi. The measured permeability values are shown in **Fig. 24**.

A change of 7% is observed in the values of permeability over the entire period of measurement although no particular trend can be observed.

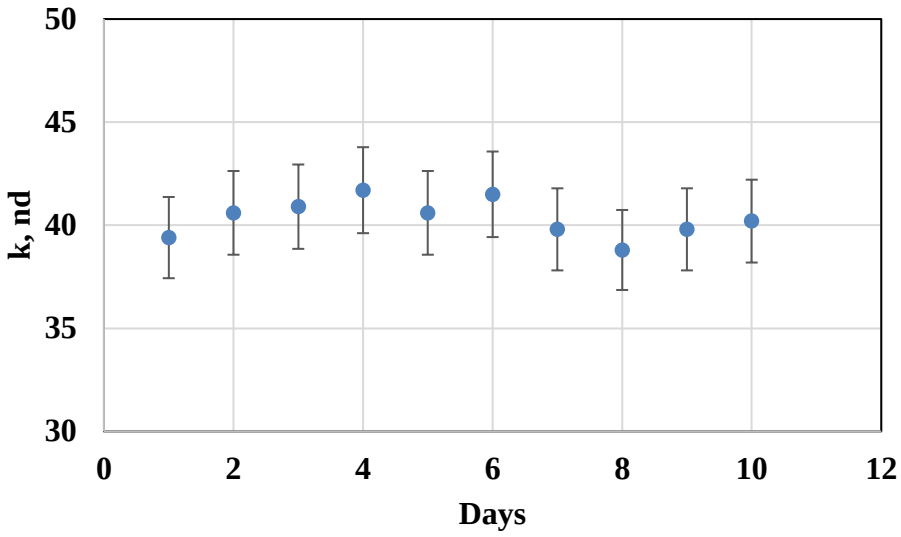

Figure 24: Measured permeability of Bakken (Upper Three Forks) sample XXX37 over a period of 10 days at an effective pressure of 3000 psi. A change of 7% is observed in the values of permeability over the entire period of measurement although no particular trend pointing to a correlation can be observed. The variation of temperature of the duration of measurement was minimal.

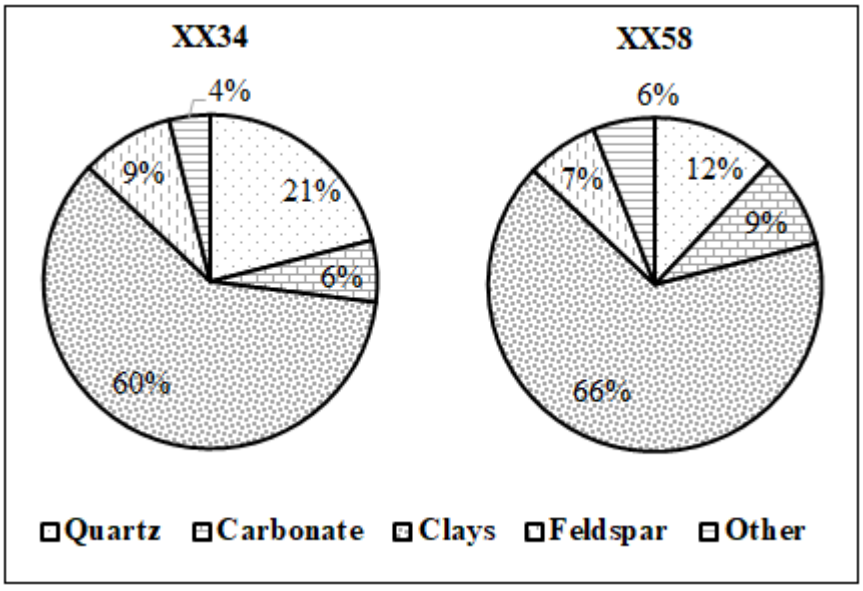

Figure 25: FTIR mineralogy for samples XX34 and XX58 (Wolfcamp).

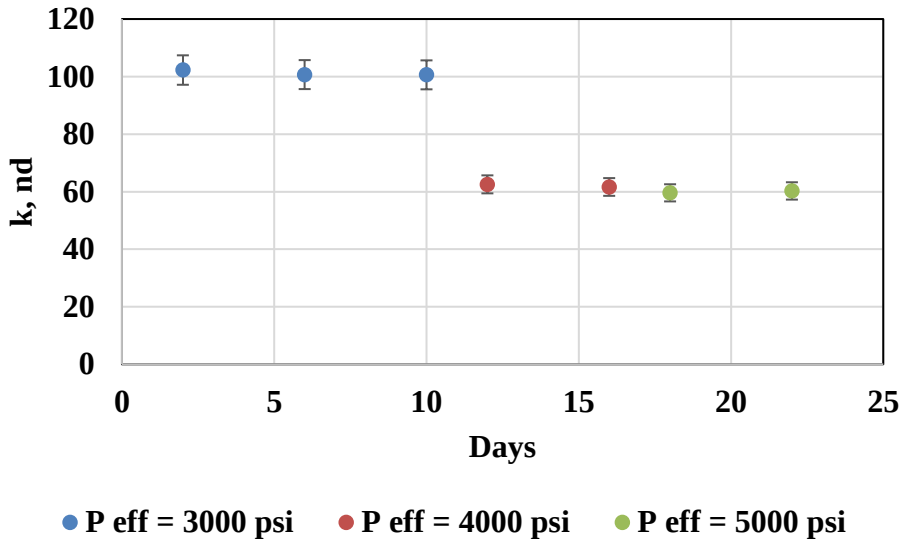

Figure 26: Permeability creep test on Wolfcamp sample XX34 at successively higher effective pressures ranging from 3000 psi to 5000 psi. The change in permeability at each effective pressure is insignificant. Permeability reduces at increasing net effective stress.

The FTIR mineralogies for Wolfcamp samples XX34 (oil window) and XX58 (oil window) are shown in **Fig. 25.** The TOC of the samples is 4.6 wt.% and 2.5 wt.% and helium porosity 6.9% and 3.5%, respectively. For Wolfcamp sample XX34 (**Fig. 26**), the average permeability at net effective stress of 3000 psi is 101 ± 5 nd. At an effective pressure of 4000 psi, permeability reduces by 39% to 62 ± 3 nd and further reduces to 59 ± 3 nd at an effective pressure of 5000 psi. The change in permeability value at each pressure stage is negligible.

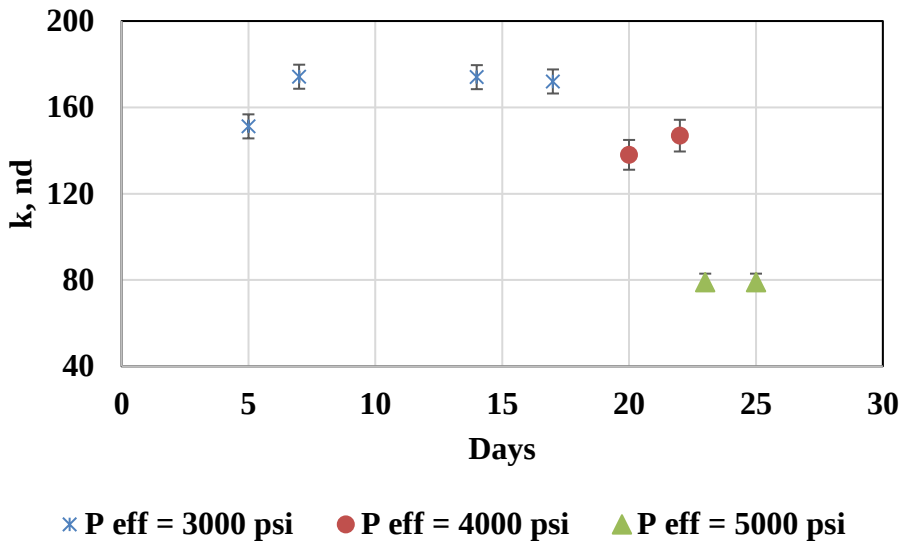

Figure 27: Permeability creep test on Wolfcamp sample XX58 at successively higher effective pressures ranging from 3000 psi to 5000 psi. The change in permeability at each effective pressure is insignificant. Permeability reduces at increasing net effective stress.

For Wolfcamp sample XX58 (**Fig. 27**), the average permeability at net effective stress of 3000 psi is 168 ± 8 nd. At an effective pressure of 4000 psi, the permeability reduces by 19% to 142 ± 7 nd and further reduces to 79 ± 4 nd at an effective pressure of 5000 psi (46% reduction). The change in permeability value at each pressure stage ranges from 15% to negligible.

For all three samples, using nitrogen for XXX37 (Bakken - Upper Three Forks) and dodecane for XX34 (Wolfcamp) and XX58 (Wolfcamp) the change in permeability over a time period of up to 10 days is insignificant (<15%). For the Wolfcamp sample (XX58), the permeability reduces with increase in effective pressure; however, the permeability variation at each effective pressure does not change significantly (<12%).

These results indicate that the long-term reservoir performance due to permeability creep, using either liquid or gas as permeant is insignificant. This is in agreement with previous

findings on shale (Mathur, 2016 and Yashura et. al., 2012). As expected, permeability reduction is observed at increasing net effective stress (pore pressure has been kept constant). Furthermore, laboratory permeability measurement time can be kept to a minimum and 'stress aging' of the sample, i.e. keeping the sample under net effective stress prior to measurement (Chhatre et al., 2014) may not be necessary. However, this may vary with sample maturity and pore fluids.

4.1.3 Effect of Temperature

Permeability of four samples, one Marcellus, two Vaca Muerta and one Wolfcamp were studied at elevated temperatures.

The method involved drying each sample for 24 hours at 212 °F before the permeability measurement to remove free water. Thereafter the permeability of the sample was measured at room temperature (~76 °F) using nitrogen as the pore fluid at net effective stress of 0.5 psi/ft.

The temperature was raised to 158 °F, using silicon heating tapes at the source (upstream section), sink (downstream section) and the test cell itself. Temperature was maintained to within ±2 °C of the set temperature using a controller. The permeability measurement at elevated temperature was performed after the system temperature stabilized.

After the system cooled to room temperature, a second set of permeability measurement was performed to ascertain if temperature related effects, if any, were irreversible.

For the four samples studied TOC lies between <1 – 5 wt. %, while the porosity ranges between 3 – 8%. The Marcellus sample was from the gas window, the Vaca Muerta

samples are from the condensate window, while the Wolfcamp sample was from the late-oil to condensate window.

The FTIR mineralogy for these samples is shown in **Figure 28**.

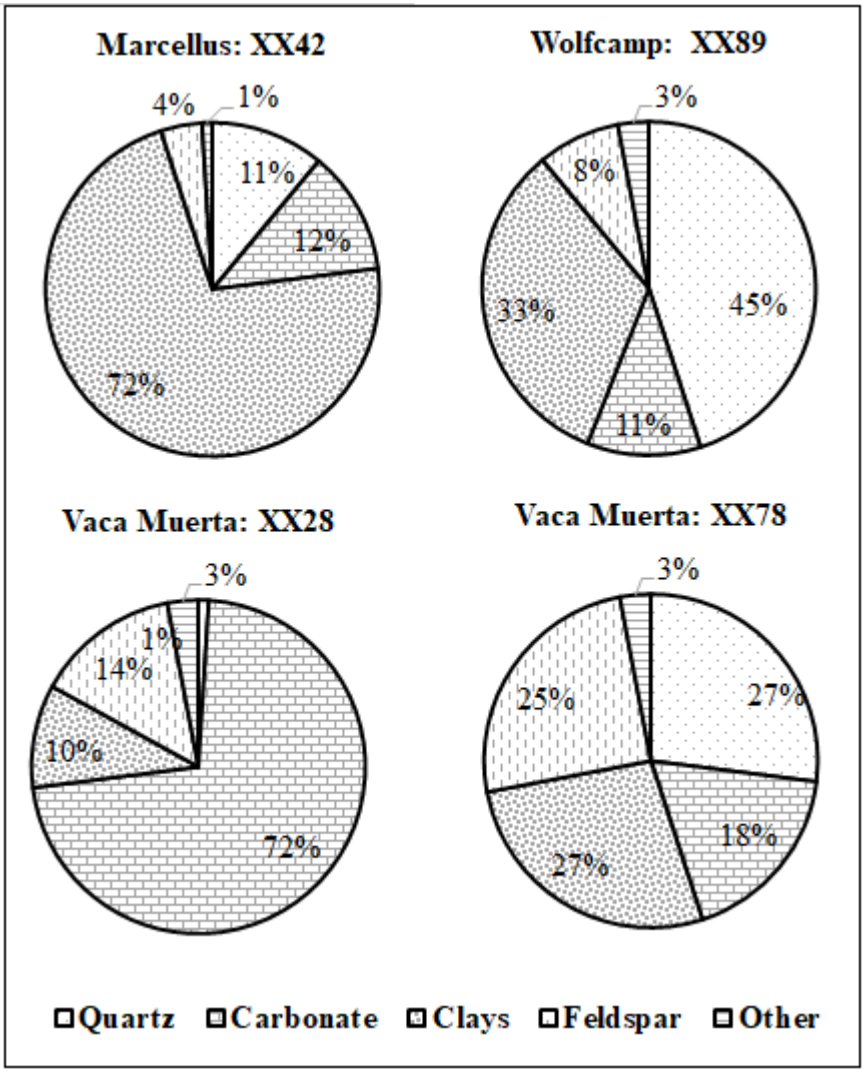

Figure 28: FTIR mineralogy of the four samples used for studying the effect of temperature on permeability measurement.

The permeability at elevated temperature of 158 °F changed by ~10% for all four samples. The second set of room temperature permeability measurements showed a difference of less than 6 % compared to the original room temperature measurements (**Fig. 29**).

The effect of temperature over the range studied on permeability of core plugs from Marcellus, Wolfcamp and Vaca Muerta formations is insignificant.

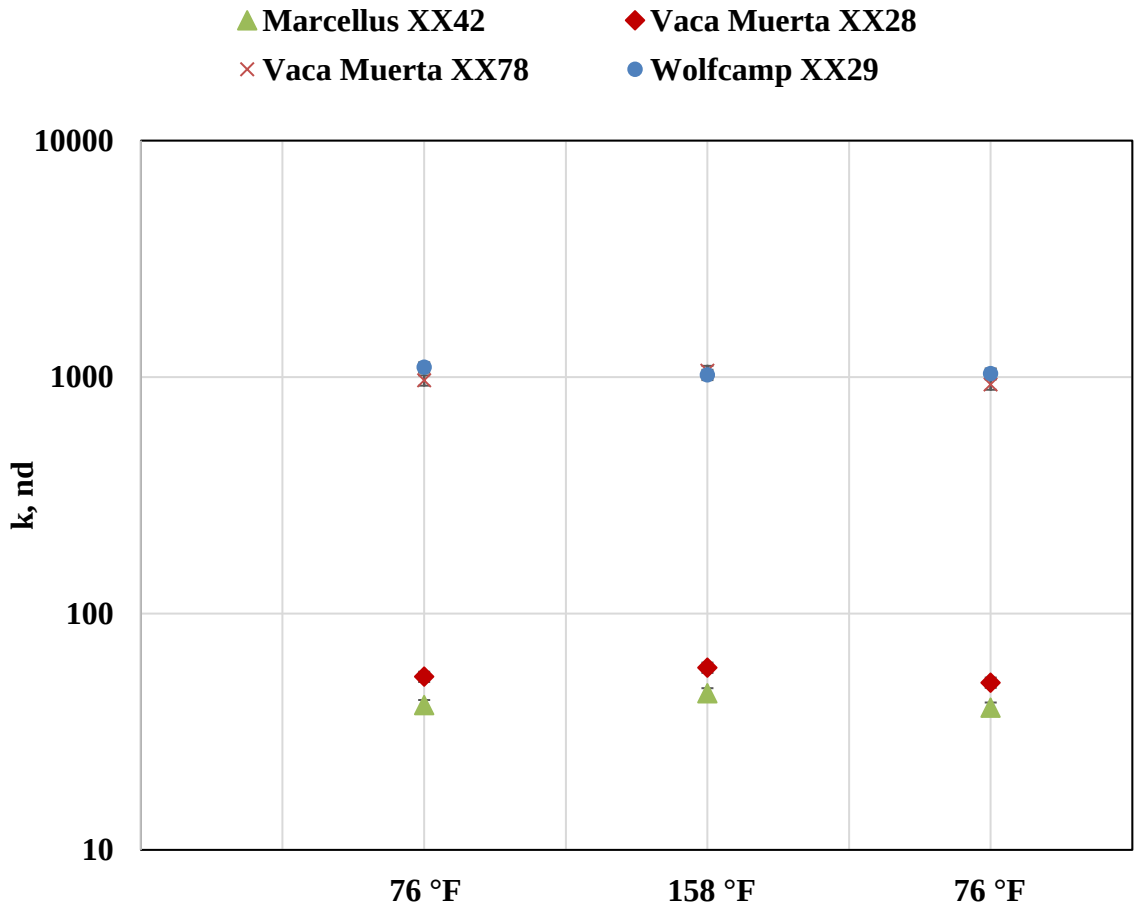

Figure 29: Permeability of 4 samples at room temperature (initial), elevated temperature and room temperature (after cooling down). Permeability at the elevated temperature changes by ~10% for all 4 samples.

The measured samples had different mineralogies (carbonate rich to clay rich) and porosity ranging from 3% to 8%. The TOC of the samples ranged between 1 and 5 wt.%.

No sensitivity is observed to any of the aforementioned properties. There are no thermodynamic or mechanical effects that cause the permeability to change within the range of temperature studied. Permeability measurements may thus be carried out at room temperature for a majority of shale formation. This contrasts with the findings of Sinha et al. (2013) who indicated that permeability of shale samples reduced by up to 25% at 230 °F compared to the room temperature steady state measurement.

As discussed in Chapter 3, while heating the samples from ambient room temperature to the elevated measurement temperature (158 °F), the test cell configuration allowed expansion of the core plug. Furthermore, the samples were dried prior to measurements to allow for removal of free water. Any thermodynamic effects owing to change in viscosity of the permeant are accounted for by using its measured viscosity at the pressure and temperature conditions of the experiment.

Permeability measurements while sensitive to the choice of pore fluid, show insignificant creep and negligible dependence on temperature.

4.2 Two Phase Flow in Shales

4.2.1. Flow of oil through a water saturated sample

The flow of oil (dodecane) through a water saturated sample was studied on a core plug from Lower Bakken formation (XXX66) from the oil window. The helium porosity of the sample was 5.5% and its TOC was 8.1 wt. %. The FTIR mineralogy of the sample is shown in **Figure 30**.

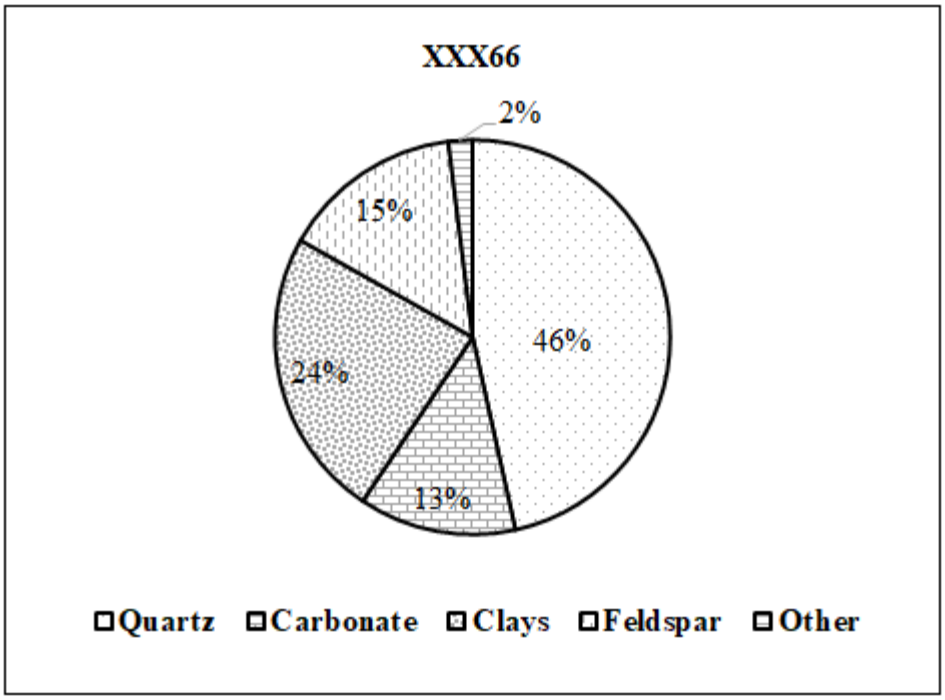

Figure 30: FTIR mineralogy of sample XXX66 from the Lower Bakken formation.

The sample was cleaned using pressurized solvent extraction using a toluene\methanol mixture. The sample was then saturated with heavy water (deuterium oxide – D_2O) at 5000 psi for 48 hours. Dodecane was flowed through the sample at an effective pressure of 3000 psi and pore pressure of 2000 psi. T_2 NMR spectrum of the sample was recorded at the following three stages to determine its saturation state:

1. After cleaning the sample using toluene\methanol mixture (at 230 °F).
2. After saturating the sample with heavy water (at 5000 psi for 48 hours).
3. After flowing dodecane through the sample at effective pressure of 3000 psi (>1 pore volume).

Fig. 31 shows the cumulative porosity from NMR (2 MHz, τ = 57 usec) data for sample XXX66 (Lower Bakken). Cumulative porosity of the cleaned sample is indicated by the curve 'Post Sohxlet' (diamond marker). Cumulative porosity recorded after saturating the sample with heavy water is indicated by 'Post D_2O' (triangular marker). The curve ('Post Dodecane') indicates the cumulative porosity recorded after the sample is saturated by dodecane at 2000 psi (square marker). The bulk volume of the sample is ~14 cm^3. The amount of heavy water that enters the sample is recorded by measuring the weight of the sample before and after saturation. In this case 0.69 g of heavy water (ρ = 1.1 gm/cm^3), or 0.62 cm^3 of it enters the sample. The heavy water porosity is thus calculated as ~4.4%. The indicated porosity however, is only ~3.5%. Upon flowing dodecane at 2000 psi pore pressure, the cumulative porosity of dodecane is ~4.5%. This represents the increase in incremental porosity. Thus, the fraction of pore volume that dodecane enters is only about 1%. This can possibly indicate that dodecane is not entering the major pore network, or it is by-passed through a crack or fracture network. The sweep efficiency of dodecane is poor.

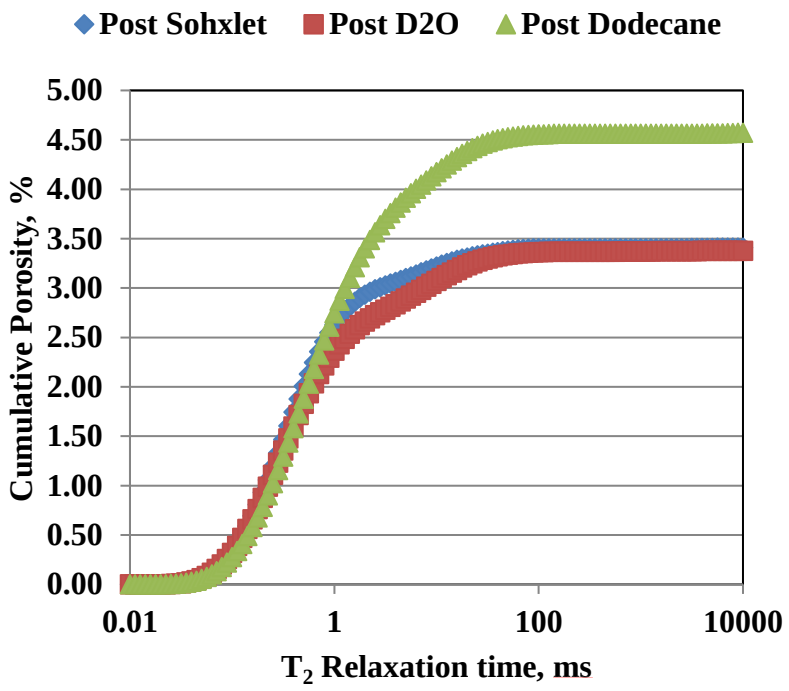

Figure 31: The NMR T_2 cumulative porosity plot for Lower Bakken sample XXX66 at three stages – after cleaning (diamond marker), after saturating with heavy water (square marker) and after saturating with dodecane (triangular marker).

Heavy water is used to saturate the sample because it is expected to have a negligible NMR signature. This allows quantification of pore volume occupied by dodecane while heavy water acts as a 'silent' background. This usage of heavy water for dodecane saturation determination using NMR has been discussed in section 3.2.

Flow behavior of dodecane in Lower Bakken sample XXX66 indicates that the displacement efficiency of dodecane is poor. In this subsequent test, the pore pressure of dodecane was successively increased and the changes in the magnitude of permeability were recorded. Two additional Bakken samples, XXX51 (Middle) and XXX14 (Three Forks) from the oil window, were used to measure the change in permeability with

increasing oil (dodecane) saturation. The helium porosity for the samples is 3.5% and 6.4%, respectively, while the TOC is 0.3 and 1.1 wt. %. The FTIR mineralogy for both the samples is shown in **Figure 32**.

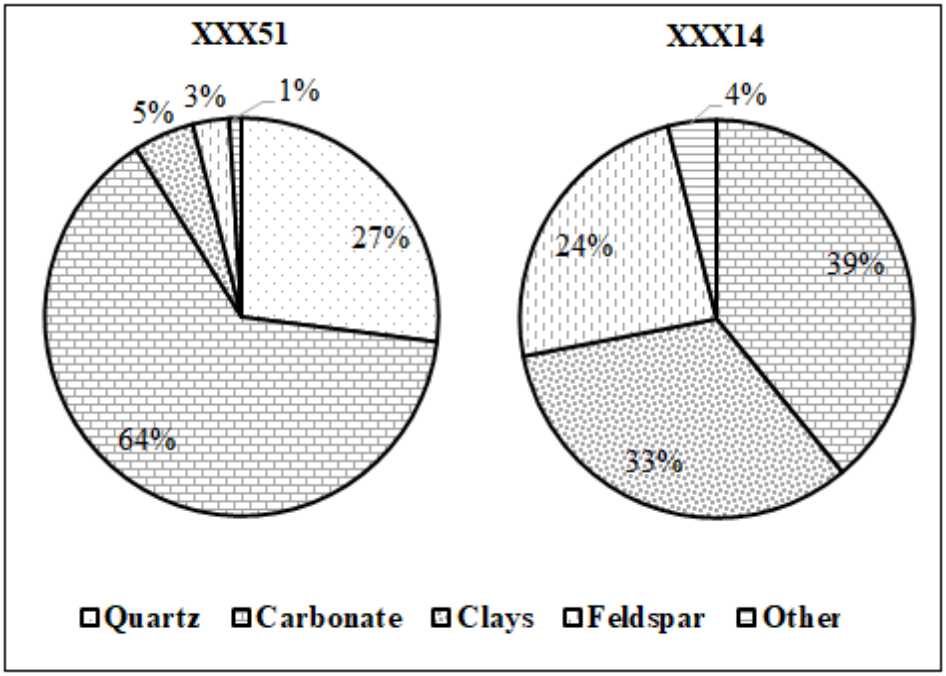

Figure 32: FTIR mineralogy of Bakken samples (Middle) XXX51 and (Three Forks) XXX14.

The samples were cleaned using pressurized solvent extraction with a toluene\methanol mixture at 1100 psi and 230 °F. Both samples were saturated with heavy water (D_2O) for a period of 48 hours at 5000 psi. The permeability of samples was recorded at successively higher pore pressures by flowing dodecane at a pore pressure of 2000 psi, 3000 psi and 4000 psi while keeping the effective pressure constant at 3000 psi. The saturation of dodecane based on the NMR cumulative porosity was recorded after flow of at least one pore volume through the core plug.

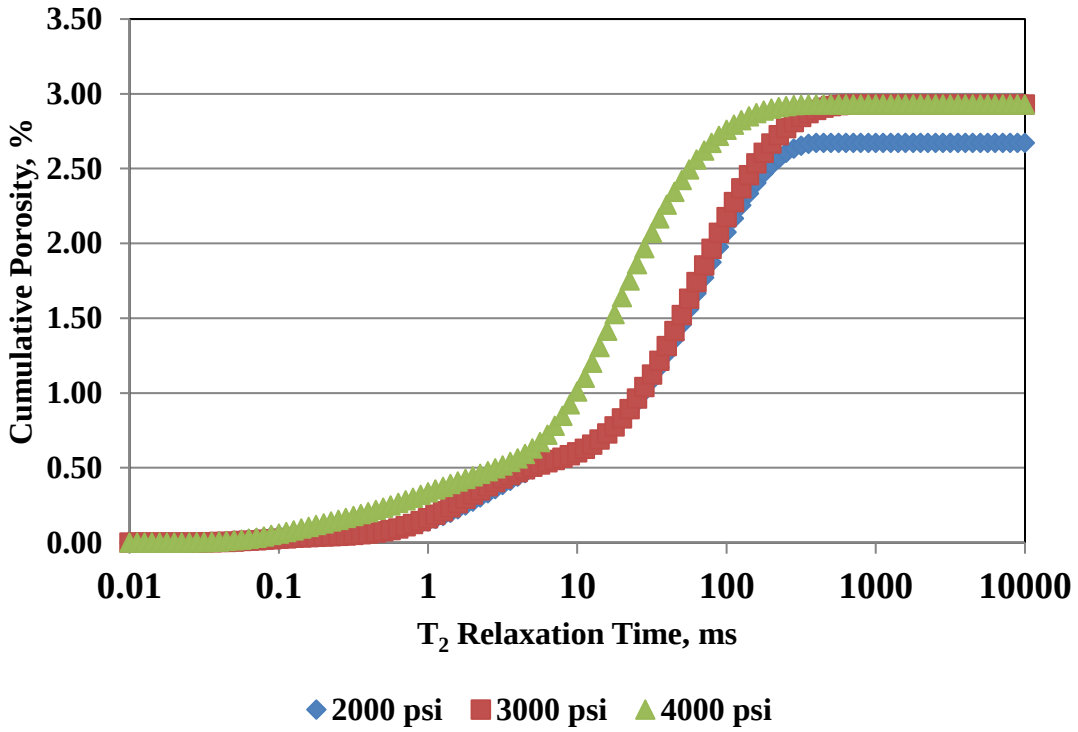

Figure 33: The NMR T_2 cumulative porosity plot for Middle Bakken sample XXX51 after flowing dodecane at 2000, 3000 and 4000 psi pore pressure (constant effective pressure = 3000 psi). An increase in the saturation of dodecane is seen with increasing pore pressure.

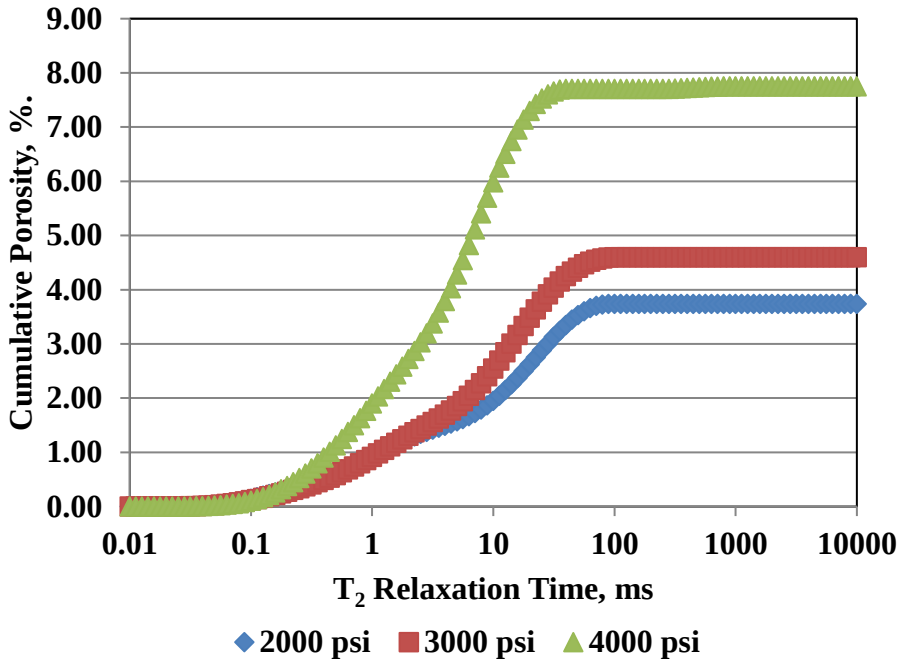

Figure 34: The NMR T_2 cumulative porosity plot for Bakken (Three Forks) sample XXX14 after flowing dodecane at 2000, 3000 and 4000 psi pore pressure (constant effective pressure = 3000 psi). An increase in the saturation of dodecane is seen with increasing pore pressure.

The permeability of dodecane through the heavy water saturated sample increases with increasing pore pressure. The saturation of dodecane, measured after flow-through at each pore pressure increases with successively higher pore pressure (**Figs. 33 and 34)**.

The increased permeability at higher pore pressure (**Fig. 35**) can possibly be attributed to dodecane entering into more pore space accessible at increasing pore pressures. The increase in saturation in smaller pores with increasing dodecane saturation suggests that dodecane channels into pores unavailable at lower pore pressures.

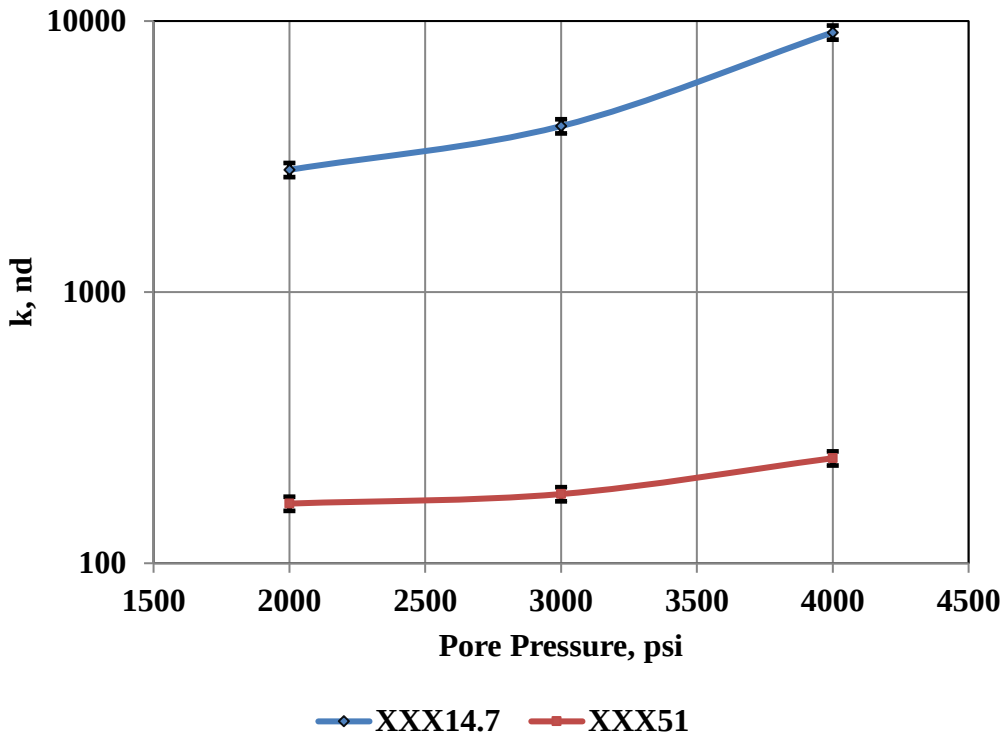

Figure 35: Change in dodecane permeability for samples XXX14 and XXX51 (Bakken/Three Forks formation) as a function of increasing pore pressure from 2000 to 4000 psi (constant effective pressure = 3000 psi, ΔP_{pore} = 100 psi). An increase in permeability is seen for both the samples with increasing pore pressure.

4.2.2 Flow of gas through a water saturated sample

The flow of gas (nitrogen) through a water saturated sample was studied on two core plugs from Utica formation. Both samples had low porosity (1 – 2%), low TOC content (~1 wt. %) and were from the condensate window. The FTIR mineralogy of the samples is shown in **Fig. 36**.

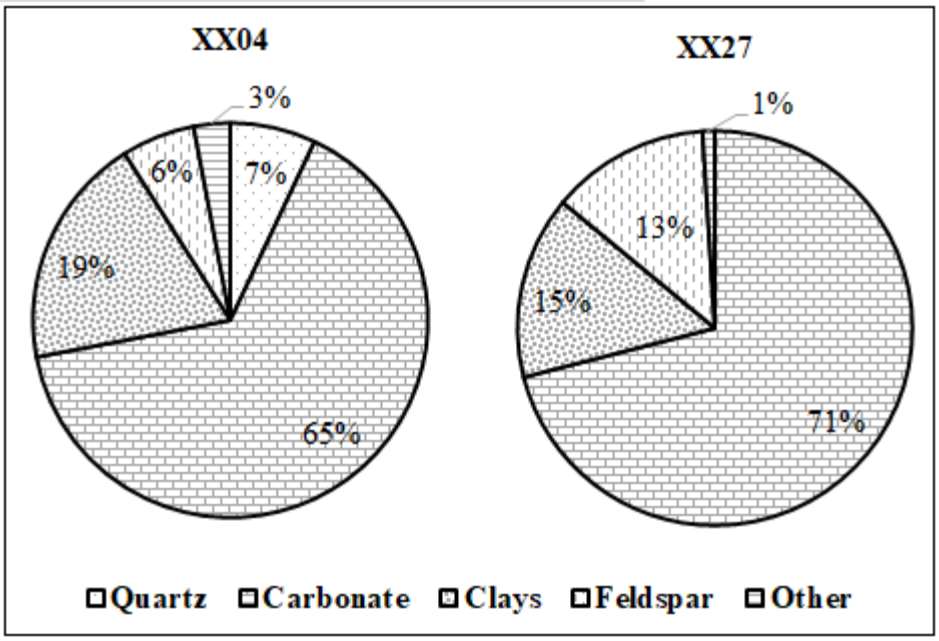

Figure 36: FTIR mineralogy of sample XX04 and XX27 from the Utica formation.

For this experiment involving flow of gas through a water saturated sample, the following steps were followed:

1. The initial 'reference' gas permeability (using N_2) of the sample at 2000 psi pore pressure and an effective pressure of 3000 psi was recorded (ΔP_{pore} = 100 psi). T_2 NMR (2 MHz, τ = 57 µs) spectrum of the sample was recorded before and after the permeability measurement. A reduction in the water saturation was observed for both Utica samples: ~6% in XX04 and ~26% in XX27.
2. The sample was saturated with brine (2.5% KCl) for 48 hours at 5000 psi. T_2 NMR spectrum of the sample was recorded (**Fig. 37(a) and 38(a)).**
3. Permeability measurements were done at the aforementioned pressure conditions and the changes in permeability were recorded as function of water saturation. The water saturation at each stage was measured using NMR (**Fig. 37(b) and 38(b)**).

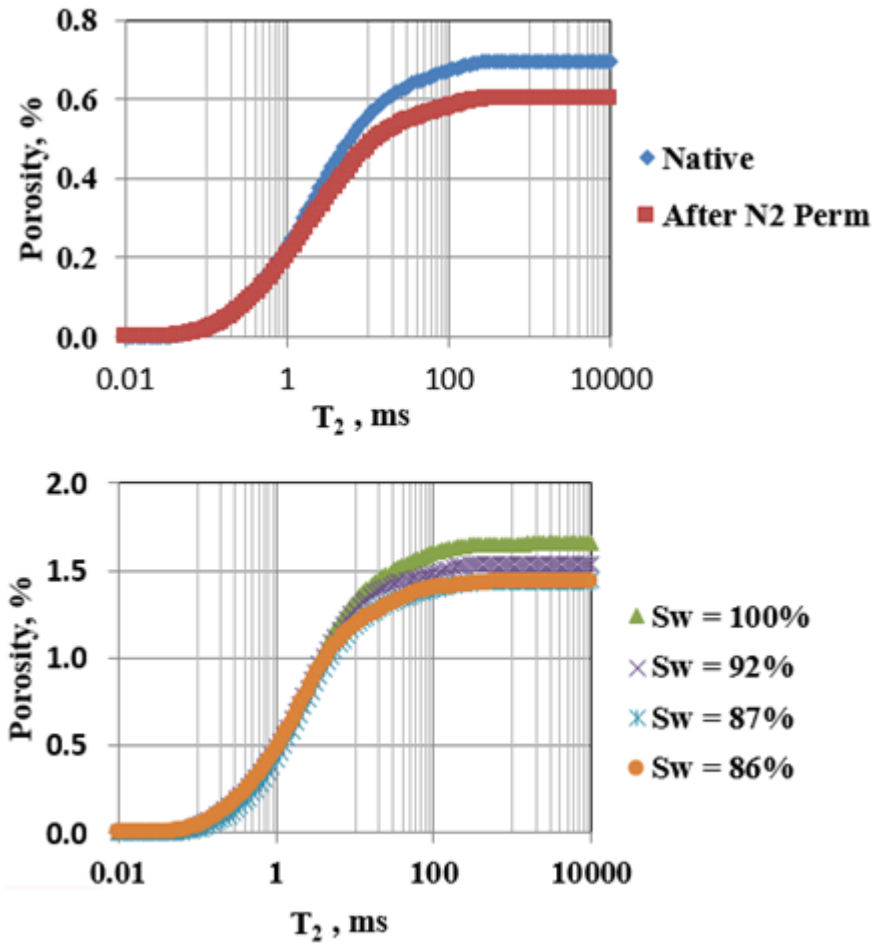

Figure 37: T_2 NMR cumulative porosity plot for Utica sample XX04, at (a) The 'as received' or 'native' saturation and after flowing N_2 to obtain the reference gas permeability and (b) the cumulative porosity after completely saturating the sample and at subsequent stages. Nitrogen is flowed through the sample at each stage for permeability measurement. A decrease in water saturation can be seen at each successive stage.

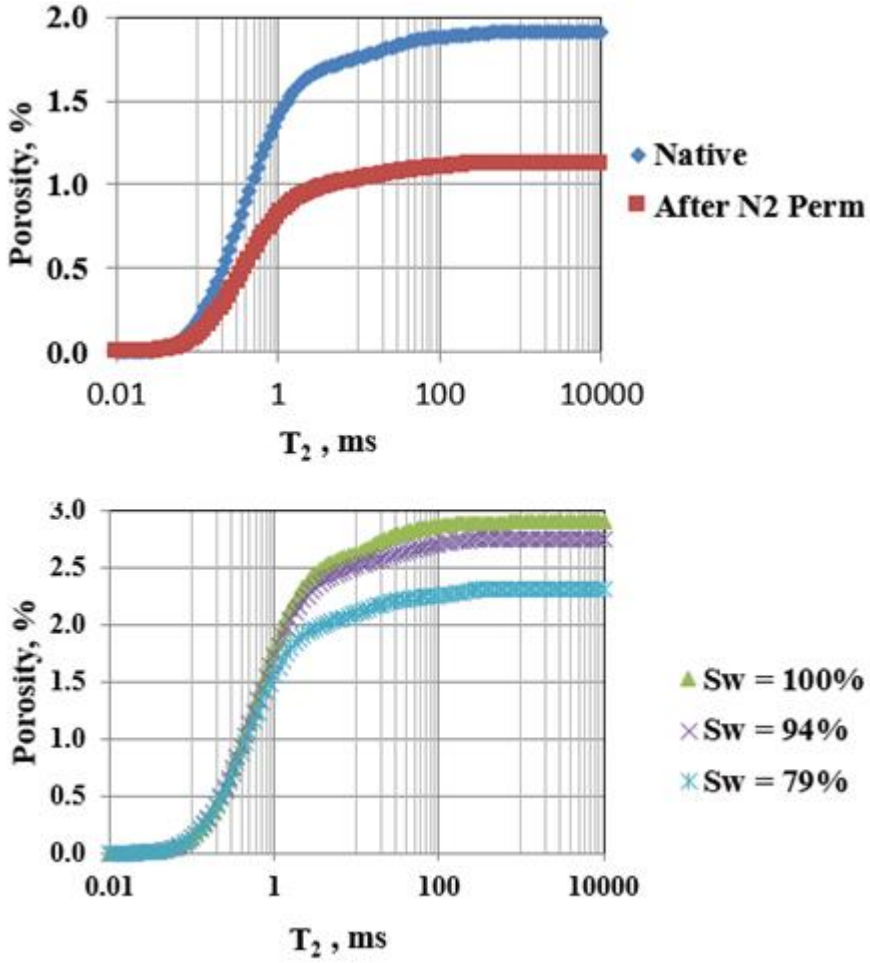

Figure 38: T_2 NMR cumulative porosity plot for Utica sample XX27, at (a) The 'as received' or 'native' saturation and after flowing N_2 to obtain the reference gas permeability and (b) the cumulative porosity after completely saturating the sample and at subsequent stages. Nitrogen is flowed through the sample at each stage for permeability measurement. A decrease in water saturation can be seen at each successive stage.

For Utica sample XX04, the nitrogen permeability was measured as 2.8 ± 0.1 µd. This was considered as the native permeability of the sample. The 'native' water saturation at this stage (after the initial permeability measurement) was 36%. After saturating the sample with water (100%) and subsequently measuring nitrogen permeability, the

saturation decreased to 92%, 87% and 86% at successive stages, corresponding to permeability values of 5.5 ± 0.27 µd, 2.0 ± 0.04 µd and 0.28 ± 0.01 µd, respectively. At each successive permeability measurement, more than one pore volume of nitrogen was flowed through the sample. The gas permeability increases with decreasing water saturation at each step (**Fig. 39**). For sample XX04, the permeability at stage 1 (i.e. S_w = 92%) the measured permeability is actually greater than the 'as received' permeability of the sample. This may be attributed to stress cracking within the sample. These tests must therefore be conducted with caution; repeated changes in the stress conditions of the sample as it is removed from the test cell for saturation estimation using NMR may cause stress cracking. S_w of Utica sample XX04 is plotted against the nitrogen permeability in **Fig. 39**.

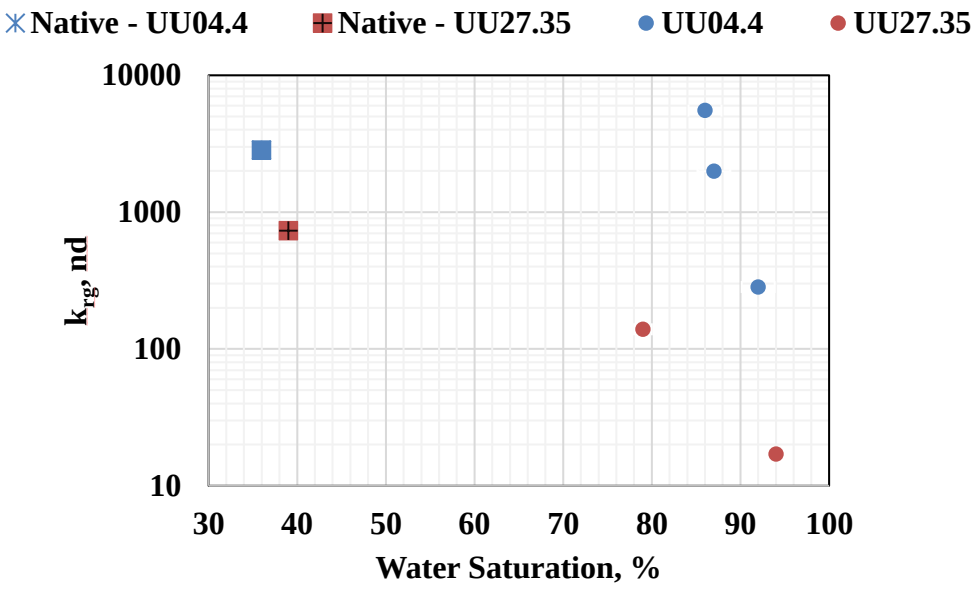

Figure 39: Steady state permeability using nitrogen plotted as function of water saturation for two samples from the Utica formation. The initial 'as is' nitrogen permeability is indicated by square markers. The subsequent values of permeability at different stages of water saturation are plotted with round markers.

Using a similar procedure for sample XX27, the value of nitrogen permeability as a function of water saturation was recorded (**Fig. 39**). The native permeability of the sample was measured as 730 ± 37 nd at S_w = 39%. The sample was saturated with brine (2.5% KCl) for a period of 48 hours at 5000 psi. Subsequently the permeability of the sample at S_w 94% and 79% was measured as 17 ± 1 nd and 139 ± 7 nd, respectively.

For both the samples, nitrogen (gas) permeability is found to increase with decreasing water saturation. The dependence of gas permeability on water saturation is nonlinear.

4.3 Permeability Estimation from MICP

Estimation of permeability using MICP data, while not precise, can be invaluable as a screening tool when whole core plugs are not available. Furthermore, permeability measurements on core plugs are typically long-duration experiments taking several days. Routine MICP measurements have thus been used to estimate the permeability of 19 shale samples which are compared to the measured steady state permeability with nitrogen as the pore fluid. The FTIR minerology of these samples from multiple formations including Bakken, Eagle Ford, Marcellus, Utica, Wilcox and Wolfcamp is shown in **Table 2**.

Table 2: FTIR Mineralogy, TOC and maturity window for samples used in estimation of permeability using MICP data

Formation	Sample	Quartz	Carb-onates	Clays	Feldspar	Other	TOC	Maturity Window
	ID	wt.%						
(Middle) Bakken	XX485	36	33	18	13	0	1.5	Oil
(Three Forks) Bakken	XX737	32	27	17	11	13	-	Oil
(Three Forks) Bakken	XX835	0	50	35	15	0	-	Oil
Eagle Ford 1	XX063	7	33	49	11	0	3.0	Dry Gas
Eagle Ford 1	XX536	0	91	5	0	4	1.0	Conden-sate
Eagle Ford 2	XX692	1	81	9	5	4	5.4	Conden-sate
Eagle Ford 2	XX721	0	42	36	10	12	4.4	Conden-sate
Marcellus	XX60	2	8	75	12	3	3.1	Dry Gas
Utica	XX81	2	28	30	5	35	1.3	Conden-sate

Utica	XX31	0	52	35	13	0	0.4	Conden-sate
Wilcox	XX11	37	10	43	9	1	1.2	-
Wolfcamp 1	XX65	61	12	7	20	0	0.4	Late Oil to Cond-ensate
Wolfcamp 1	XX83	43	19	25	12	1	1.4	Late Oil to Cond-ensate
Wolfcamp 1	XX87	27	17	19	32	5	0.7	Late Oil to Cond-ensate
Wolfcamp 1	XX07	45	5	25	24	1	0.7	Late Oil to Cond-ensate
Wolfcamp 1	XX01	59	3	23	12	3	1.4	Late Oil to Cond-ensate
Wolfcamp 2	XX40	22	6	62	6	4	2.0	Oil
Wolfcamp 2	XX12	11	15	60	10	4	1.7	Oil
Wolfcamp 2	XX48	6	16	56	17	5	2.0	Oil

Permeability estimation from MICP data has been evaluated using the following methods: (a) Kozeny equation, (b) Winland's method, (c) Swanson's method, (d) Thomeer's method and (e) Katz Thompson method.

Kozeny equation relates the permeability of a porous medium having porosity 'Φ' consisting of a bundle of tubes with radius 'r'. The point on the capillary pressure curve where 35% saturation of Hg is achieved has been designated as $r_{35.}$ Using the aforementioned parameters, the permeability of the samples has then been estimated using **Equation 8**.

$$\mathbf{k = \emptyset \frac{r_{35}^2}{8} * 1.01325 * 10^3} \qquad \textbf{(8)}$$

Where:

k = Permeability (nd)

∅ = Porosity (%)

r_{35} = Pore throat radius at 35% Hg Saturation (nm)

A crossplot on the log-log scale between the measured steady state permeability (x-axis) and the estimated permeability (y-axis) is shown in **Fig. 40**.

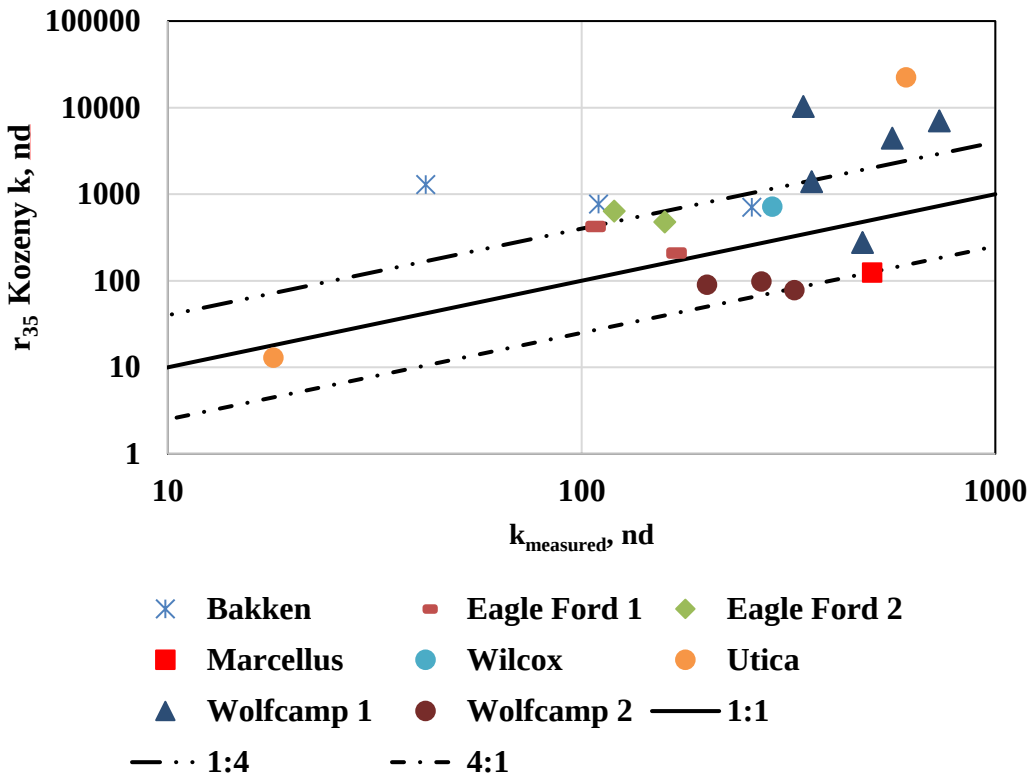

Figure 40: Crossplot between measured steady state permeability and MICP estimated permeability (using Kozeny equation – r_{35}) for 19 samples. ~60% of the estimated values lie within a factor of 4 of the measured permeability.

11 of the 19 samples, i.e. ~60% of the samples lie within a factor of 4 from the measured permeability.

Using **Equation 8** but employing r_{max}, i.e. the peak of the incremental mercury volume plotted against pore throat radius, 13 of 19 samples, i.e. ~70% of the samples lie within a factor of 4 of the measured permeability (**Fig. 41**).

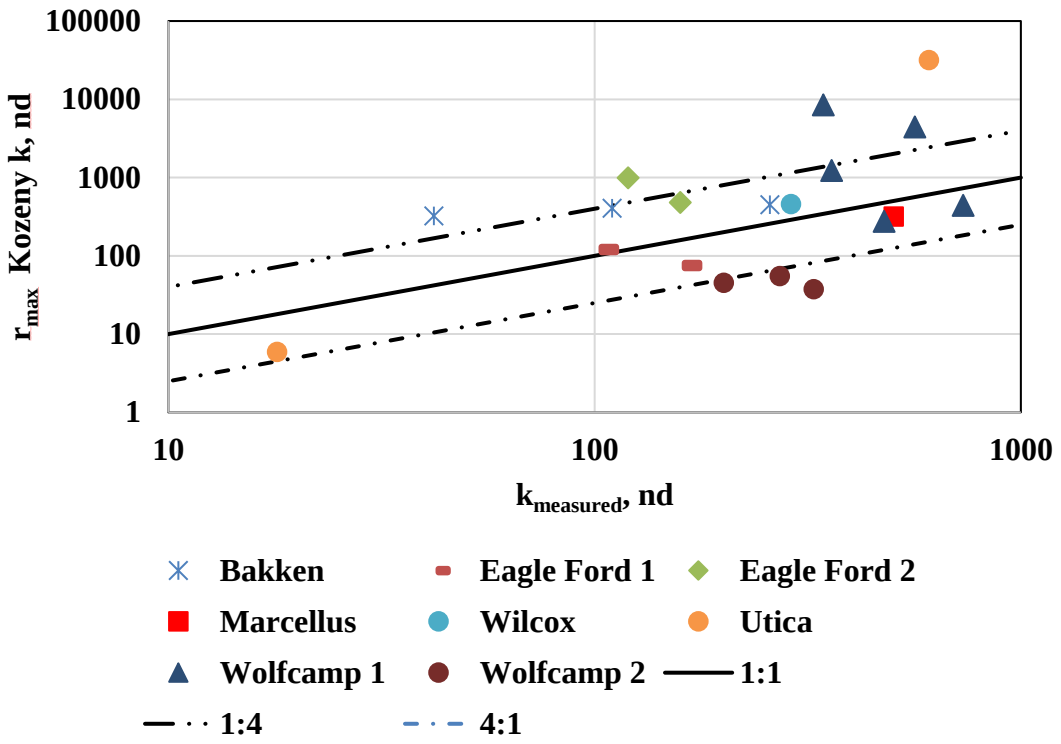

Figure 41: Crossplot between measured steady state permeability and MICP estimated permeability (using Kozeny equation - r_{max}) for 19 samples. ~70% of the estimated values lie within a factor of 4 of the measured permeability.

Winland (Pittman,1992) built a correlation between porosity and r_{35} values of 82 sandstone and carbonate samples with slippage corrected measured permeability as well as an additional 240 samples without any slippage corrections. The permeabilities for these samples were measured at ambient pressure conditions of 800 – 1000 psi (Comisky et al., 2007). This correlation (**Equation 9**) has also been used to estimate the permeability of shale samples. Only six of 19 samples studied have the estimated permeability within a factor of 4 of the measured steady state permeability (**Fig. 42**)

$$\log(r_{35}) = 0.732 + 0.588\log(k_{winlandair}) - 0.864\log(\emptyset) \quad (9)$$

Where:

r_{35} = Pore throat radius at 35% Hg Saturation (nm)

k_{air} = Permeability estimated from Winland's correlation (nd)

$\emptyset$ = Porosity (%)

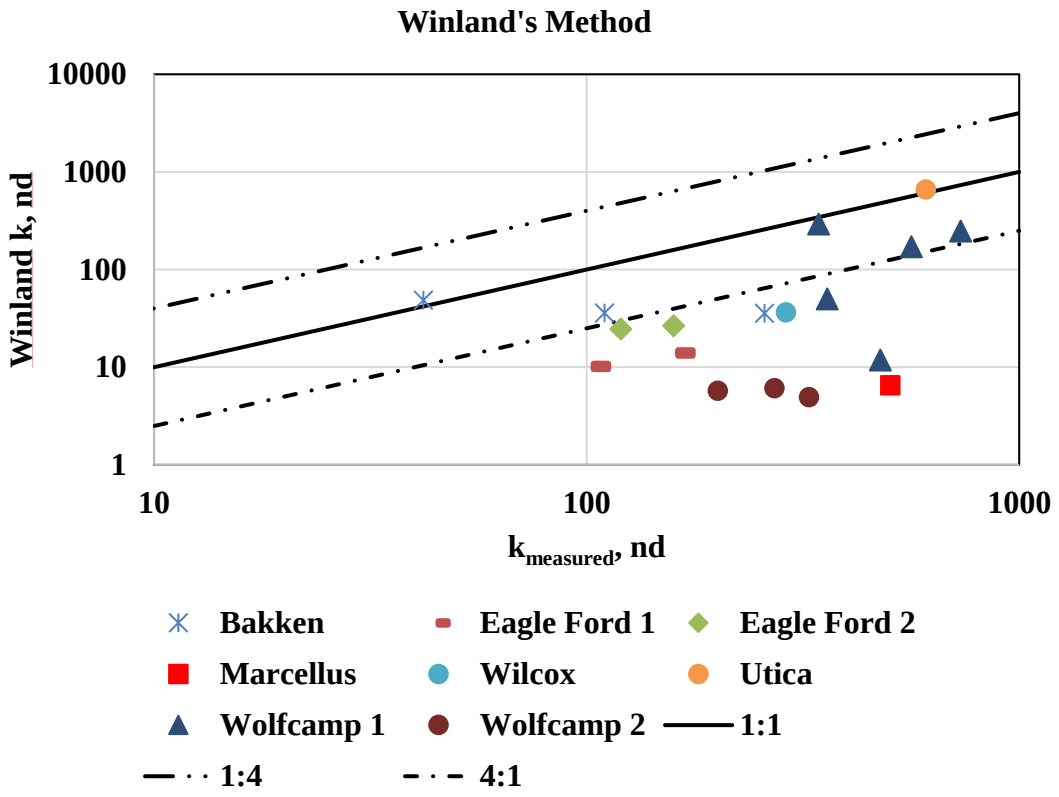

Figure 42: Crossplot between measured steady state permeability and MICP estimated permeability (using Winland's equation) for 19 samples. ~30% of the estimated values lie within the a factor of 4 of the measured permeability.

The apex of (S_b/P_c) plot is a point where the permeability controlling major connected pore spaces were saturated with mercury (**Fig. 43**). Swanson (1981) formulated an empirical relation (**Equation 10**) based on measurements on 319 samples (sandstones

and carbonates). The net confining stress on these samples was between 800 - 1000 psi (Comisky et al., 2007).

$$k_{Swanson} = 399 \left(\frac{S_b}{P_c}\right)^{1.691} \quad \textbf{(10)}$$

Where:

$k_{Swanson}$ = Swanson permeability (md)

S_b/P_c = Hg saturation (% of bulk volume)/Capillary Pressure at Apex

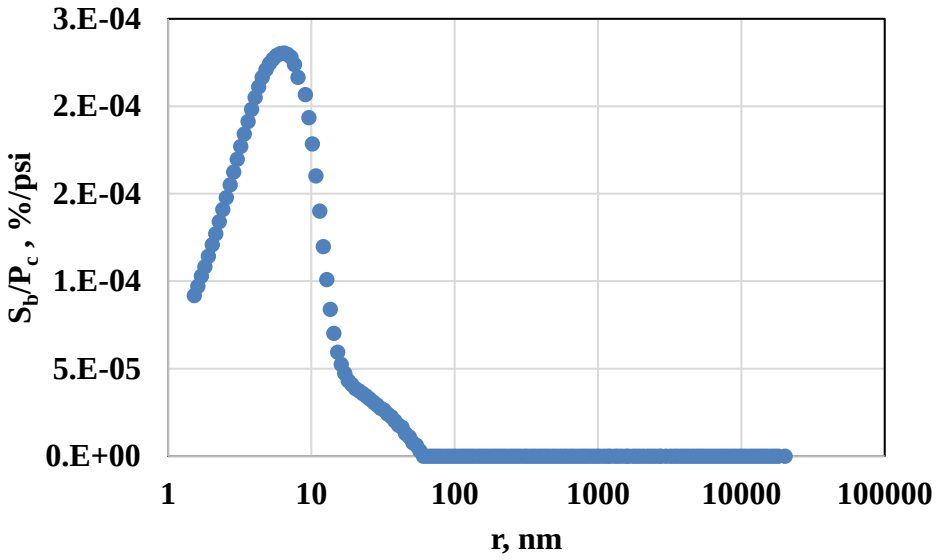

Figure 43: Apex plot for a Wilcox formation sample (XXSH) using Swanson's method. The apex of (S_b/P_c) is indicative of the point where the permeability-controlling pore spaces are connected.

The estimated permeability using Swanson's method for Wilcox sample (XXSH) is 282 nd, which is nearly equal to the measured steady state permeability (289 ± 14 nd).

The permeability of 19 samples was estimated this method (**Fig. 44**). 12 of 19 samples, i.e. ~65% of the samples have estimated permeability within a factor of 4 of the measured steady state permeability.

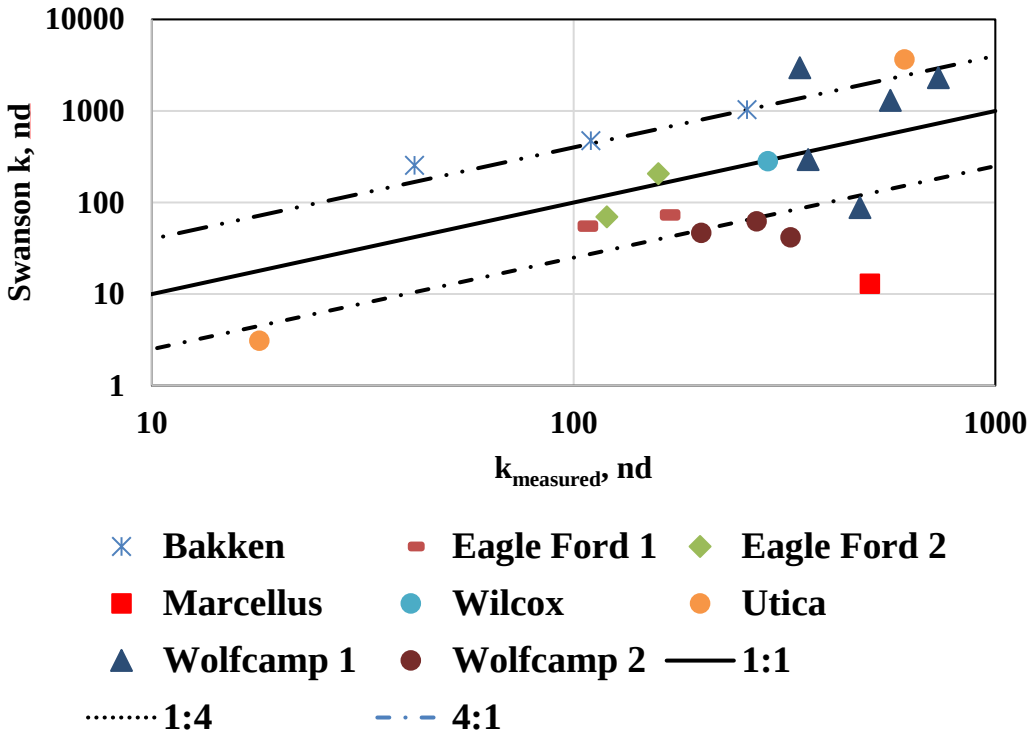

Figure 44: Crossplot between measured steady state permeability and MICP estimated permeability (using Swanson's method) for 19 samples. ~65% of the estimated values lie within a factor of 4 of the measured permeability.

Thomeer (1960; 1983) showed that mercury capillary pressure curve can be uniquely defined by a hyperbola with three specific factors quantifying its shape and asymptotes (**Equation 11**).

$$\mathbf{k_{Thomeer}} = \mathbf{3.81}\, F_g^{-1.33} \left(\frac{\mathbf{S_{b\infty}}}{\mathbf{P_d}}\right)^2 \qquad \textbf{(11)}$$

Where:

$k_{Thomeer}$ = Thomeer permeability (md)

F_g = Pore geometrical factor

$S_{b\infty}$ = Percentage bulk volume occupied by Hg at infinite P_C (%)

P_d : Displacement pressure, psi

The values of F_g, $S_{b\infty}$ and P_d were calculated for each sample analyzed by fitting a curve to the mercury capillary pressure data. **Fig. 45** shows the aforementioned shape factors determined for a Bakken sample. The measured steady state permeability of the sample is 258 ± 13 nd and permeability estimated using Thomeer's method for the sample is 481 nd. The estimated permeability is higher than the measured permeability by a factor of 1.86.

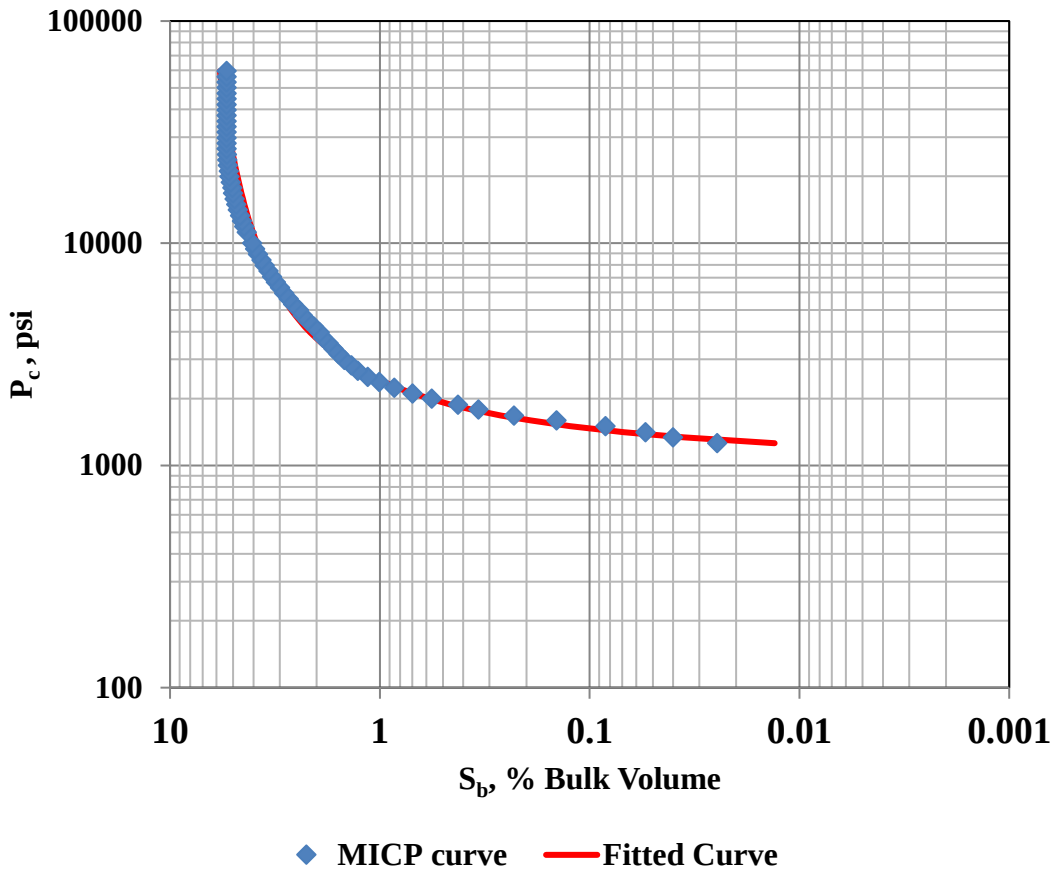

Figure 45: Determination of F_g, $S_{b\infty}$ and P_d using for a Bakken sample. The values determined have then been used to estimate the permeability of the sample as 481 nd. The measured steady state permeability value is 258 ± 13 nd.

Using Thomeer's estimation, 12 of 19 samples (~65%) have estimated permeability within a factor of 4 of the measured steady state permeability (**Fig. 46**).

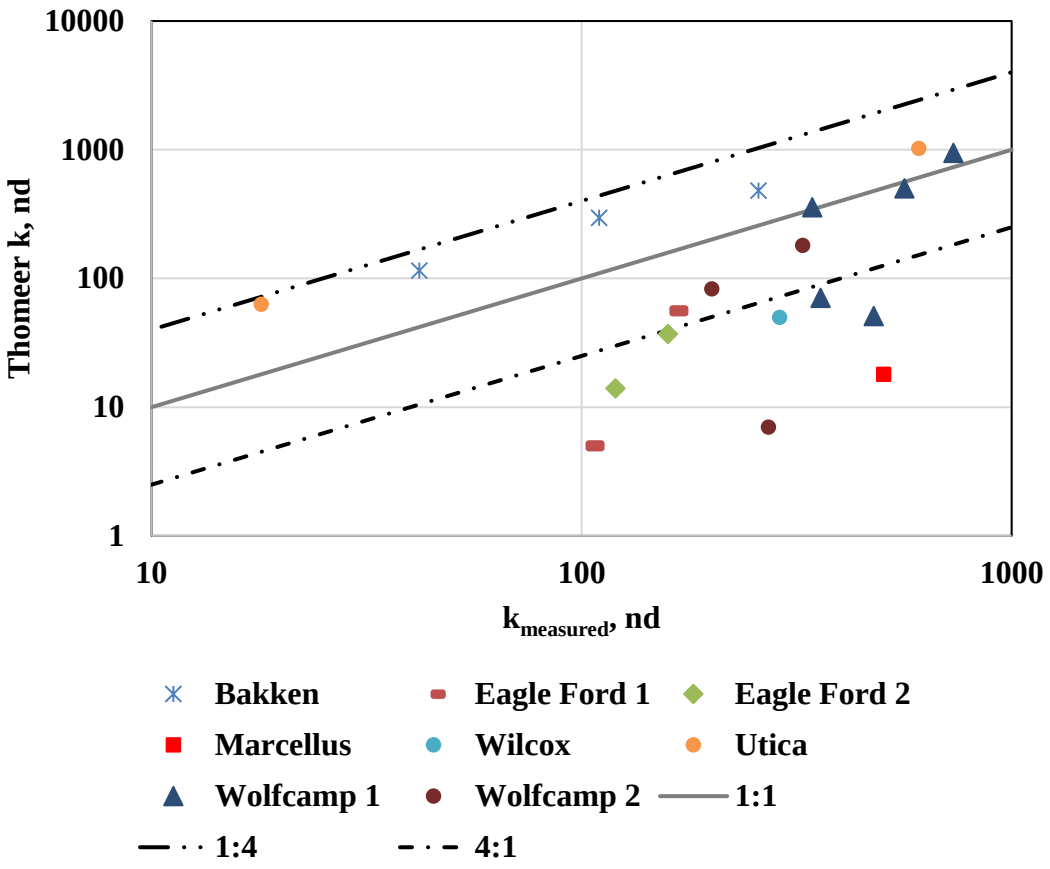

Figure 46: Crossplot between measured steady state permeability and MICP estimated permeability (using Swanson's method) for 19 samples. ~65% of the estimated values lie within a factor of 4 of the measured permeability.

Katz and Thompson (1986) characterized the fluid flow and electrical conductance through porous media using percolation theory. The fluid flow through a porous medium was defined by characteristic length (L_C) i.e. the pore diameter where the pore spaces across the sample were saturated by mercury, and maximum electrical conductance length (L_{Emax}), i.e. the pore throat diameter where the ionic conductance was maximized.

$$k_{LE} = \frac{1013}{226} * L_C^2 * \frac{L_{Emax}}{L_C} * \emptyset * S_{LEmax} \quad (12)$$

Where:

k_{LE}: Permeability, μm^2

L_C: Characteristic length, µm

L_{Emax}: Effective pore throat diameter at maximum ionic conductance, µm

Ø: Porosity, fraction

S_{LEmax}: Mercury saturation at L_{Emax}, fraction

The permeability of 19 samples estimated using Katz-Thompson method has been plotted against the measured steady-state permeability (**Fig. 47**). The estimated permeability is one to three orders of magnitude higher than the measured permeability.

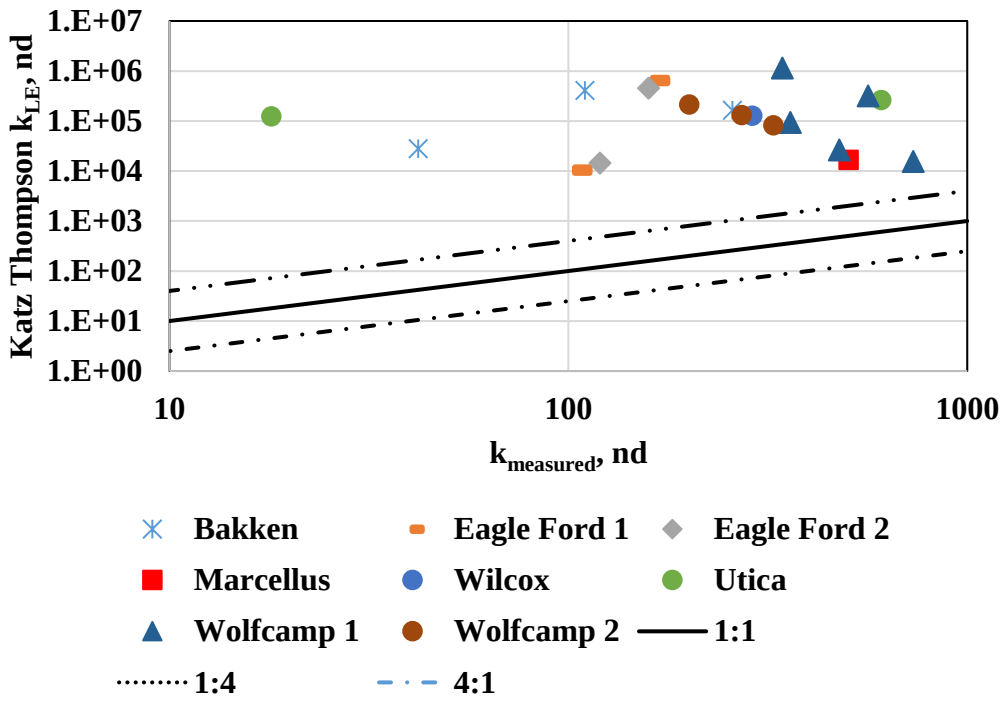

Figure 47: Crossplot between measured steady state permeability and MICP estimated permeability (using Katz-Thompson's method) for 19 samples. Estimated values are higher than measured permeability by one to three orders of magnitude.

Table 3: Predicting power of correlations studied to estimate permeability to within a factor of 4 of the measured permeability

Method	**% of samples within a factor of 4 of the measured permeability**
Kozeny (r_{35})	60
Kozeny (r_{max})	70
Winland	30
Swanson	30
Thomeer	65
Katz Thompson	0

All correlations were developed for conventional rocks, which have different pore structures than shales. A correlation based on a larger data set of shale samples can help establish a correlation better describing the permeability of that particular zone.

Using these measurements and estimating permeability values using Thomeer and Swanson methods amongst others can provide a valuable screening tool to indicate zones with low and high permeability. It can also provide a relative sense of high or low permeability within a dataset. Where core plugs are not available, drill cuttings can be used for such estimations as well. Preliminary petrophysical analysis on drill cuttings,

including estimation of permeability from MICP data, can provide valuable information for screening of productive zones.

Chapter 5: Conclusions

Three distinct studies were performed to characterize and understand matrix permeability in shales:

1. Effects of pore fluid, creep and temperature
2. Two phase flow experiments involving oil (dodecane) and gas (nitrogen) flow through water saturated samples
3. Estimation of permeability using MICP

The main conclusions are as follows:

- Measured steady-state gas permeability can be significantly higher than steady-state liquid permeability. The nitrogen permeability for Bakken, Eagle Ford, Wilcox and Wolfcamp shales are greater than the dodecane permeability by as much as a factor of 4.
- Permeability creep, i.e. change in permeability as a function of time is insignificant for Bakken (oil window) and Wolfcamp (oil window) shales.
- Permeability measurements conducted at room temperature are within 10% of the elevated temperature measurements (158° F) for Marcellus, Vaca Muerta and Wolfcamp formations.
- Gas permeability at different water saturations was determined for Utica shales. Gas permeability increases nonlinearly with decreasing water saturation.
- MICP derived permeability can serve as a screening tool to determine zones of high permeability. Using different correlations, estimated permeabilities for up to 70 % of the samples studied were within a factor of 4 of the measured permeability. For the data set used, using Kozeny equation with r_{max}, works best

to estimate the permeability within a defined range of a factor 4 times the measured permeability.

References

Bangia, V. K., Yau, F. F., and Hendricks, G. R. 1993. Reservoir Performance of a Gravity-Stable, Vertical CO_2 Miscible Flood: Wolfcamp Reef Reservoir, Wellman Unit. SPE Reservoir Eng. **8** (4). SPE-22898-PA.

Beskok, A., and Karniadakis, G. E. 1999. Report: A Model for Flows in Channels, Pipes, and Ducts at Micro and Nano Scales. Microscale Thermophysical Engineering **3**(1): 43-77.

Bello, R. O. 2009, Rate Transient Analysis in Shale Gas Reservoirs with Transient Linear Behavior. PhD thesis, Texas A&M University. (May 2009).

Brace, W. F., Walsh, J. B., and Frangos, W. T. 1968. Permeability of Granite Under High Pressure. J. Geophys. Res. **73** (6): 2225-2236.

Brezovski, R., and Cui, A. 2013. Laboratory Permeability Measurements of Unconventional Reservoirs: Useless or Full of Information? A Montney Example From the Western Canadian Sedimentary Basin. Presented at the SPE Unconventional Resources Conference and Exhibition-Asia Pacific, San Antonio, Texas, 11—13 November.

Bustin, R. M., Bustin, A. M. M., Cui, A., Ross, D., and Pathi, V. M. 2008. Impact of Shale Properties on Pore Structure and Storage Characteristics. Presented at SPE Shale Gas Production Conference, Fort Worth, Texas, 16-18 November. SPE-119892-MS.

Chhatre, S. S., Braun, E. M., Sinha, S., Determan, M. D., Passey, Q. R., Zirkle, T. E., Wood, A. C., Boros, J. A., Berry, D. W., Leonardi, S. A. and Kudva, R. A. 2014. Steady State Stress Dependent Permeability Measurements of Tight Oil Bearing Rocks. Presented at International Symposium of the Society of Core Analysts, Avignon, France, 8-11 September. SCA2014- 012.

Civan, F. 2010. Effective Correlation of Apparent Gas Permeability in Tight Porous Media. Transport in Porous Media. **82** (2): 375-384.

Comisky, J. T., Newsham, K., Rushing, J. A., and Blasingame, T. A. 2007. A Comparative Study of Capillary-Pressure-Based Empirical Models for Estimating Absolute Permeability in Tight Gas Sands. Presented at the SPE Annual Technical Conference and Exhibition, Anaheim, California, 11—14 November. SPE-110050-MS.

Cui, X., Bustin, A. M. M., and Bustin, R. M. 2009. Measurements of Gas Permeability and Diffusivity of Tight Reservoir Rocks: Different Approaches and Their Applications. *Geofluids*. **9** (3): 208-233.

Curtis, M .E., Ambrose, R. J., Sondergeld, C. H. et al. 2010. Structural Characterization of Gas Shales on the Micro-and Nano-scales. Presented at the Canadian Unconventional Resources and International Petroleum Conference, Calgary, Canada, 19—21 October. SPE-137693.

Dacy, J. M. 2010. Core Tests for Relative Permeability of Unconventional Gas Reservoirs. Presented at the SPE Annual Technical Conference and Exhibition, Florence, Italy, 19-22 September. SPE-135427-MS.

Purcell, W.R. 1949. Capillary Pressures - Their Measurement Using Mercury and the Calculation of Permeability Therefrom. Journal of Petroleum Technology **1** (2): 39—48.

Dicker, A. I., and Smits, R. M. 1988. A Practical Approach for Determining Permeability From Laboratory Pressure-Pulse Decay Measurements. Presented at International Meeting on Petroleum Engineering, Tianjin, China, 1-4 November. SPE-17578-MS.

EIA Annual Energy Outlook 2017, U.S. Energy Information Administration, January 2017, https://www.eia.gov/outlooks/aeo/pdf/0383(2017).pdf (accessed 1 April, 2017)

EIA Annual Energy Outlook 2015, U.S. Energy Information Administration, April 2015, https://www.eia.gov/outlooks/aeo/pdf/0383(2015).pdf (accessed 1 April, 2017)

Fathi, E., Tinni, A., and Akkutlu, I. Y. 2012. Shale Gas Correction to Klinkenberg Slip Theory. Presented at SPE Americas Unconventional Resources Conference, Pittsburgh, Pennsylvania, 5-7 June. SPE-154977-MS.

Guidry, F. K., Luffel. D. L., Curtis, J. B. 1996. Development of Laboratory and Petrophysical Techniques for Evaluating Shale Reservoirs, Gas Research Institute Report, GRI-5/0496.

Hagoort, J. 1980. Oil Recovery by Gravity Drainage. SPE Journal **20** (3): 139-150. SPE-7424.

Heller, R., and Zoback, M. 2013. Laboratory Measurements of Matrix Permeability and Slippage Enhanced Permeability in Gas Shales. Presented at the Unconventional Resources Technology Conference, Denver, Colorado, 12-14 August. URTEC-1582659-MS.

Hsieh, P. A., Tracy, J. V., Neuzil, C. E., Bredehoeft, J. D., and Silliman, S. E. 1981. A Transient Laboratory Method for Determining the Hydraulic Properties of 'Tight' Rocks—I. Theory. International Journal of Rock Mechanics and Mining Sciences and Geomechanics Abstracts, **18** (3): 245-252.

Jin, G., Pérez, H. G., Agrawal, G., Khodja, M. R., Ali, A. Z., Hussaini, S. R., and Jangda, Z. Z. 2015. The Impact of Gas Adsorption and Composition on Unconventional Shale Permeability Measurement. Presented at the SPE Middle East Oil and Gas Show and Conference, Manama, Bahrain,8-11 March. SPE-172744-MS.

Jones, S. C. 1997. A Technique for Faster Pulse-Decay Permeability Measurements in Tight Rocks. SPE Formation Evaluation, **12** (01): 19-26. SPE-28450-PA.

Katz, A. J. and Thompson, A. H. 1986. Quantitative Prediction of Permeability in Porous Rock. Physical Review B 34(11): 8179-8181.

Klinkenberg, L. J. 1941. The Permeability of Porous Media to Liquids and Gases. In Drilling and Production Practice. American Petroleum Institute.

Lan, Q., Xu, M., Dehghanpour, H., and Wood, J. 2014. Advances in Understanding Wettability of Tight and Shale Gas Formations. Presented at the SPE Annual Technical Conference and Exhibition, Amsterdam, Netherlands, 27-29 October. SPE-170969-MS.

Lasseux, D., Jannot, Y., Profice, S., Mallet, M., and Hamon, G. 2012. The "Step Decay": A New Transient Method for the Simultaneous Determination of Intrinsic Permeability, Klinkenberg Coefficient and Porosity on Very Tight Rocks. Presented at the International Symposium of the Society of Core Analysts, Aberdeen, Scotland, 27-30 August. SCA2012-25.

Loucks, R. G., Reed, R. M., Ruppel, S. C., and Jarvie, D. M. 2009. Morphology, Genesis, and Distribution of Nanometer-Scale Pores in Siliceous Mudstones of the Mississippian Barnett Shale. Journal of Sedimentary Research **79** (12): 848-861.

Luffel, D. L., Hopkins, C. W. and Schettler, P. D. 1993. Matrix Permeability Measurement of Gas Productive Shales. Presented at the SPE Annual Technical Conference and Exhibition, Houston, Texas, 3-6 October. SPE-26633-MS.

Mathur, A. 2015, Experimental Investigation of Matrix Permeability of Shale. MS thesis, University of Oklahoma. (August, 2015).

Mathur, A., Sondergeld, C. H., and Rai, C. S. 2016. Comparison of Steady-State and Transient Methods for Measuring Shale Permeability. Presented at the SPE Low Perm Symposium, Denver, Colorado, 5-6 May. SPE-180259-MS.

Metwally, Y. M., and Sondergeld, C. H. 2011. Measuring Low Permeabilities of Gas-sands and Shales Using a Pressure Transmission Technique. International Journal of Rock Mechanics and Mining Sciences 48 (7): 1135-1144.

Moghadam, A. A., and Chalaturnyk, R. 2015. Laboratory Investigation of Shale Permeability. Presented at the SPE/CSUR Unconventional Resources Conference, Calgary, Alberta, Canada, 20-22 October. SPE-175919-MS.

Morsy, S., Sheng, J. J., Hetherington, C. J., Soliman, M. Y., and Ezewu, R. O. 2013. Impact of Matrix Acidizing on Shale Formations. Presented at the SPE Nigeria Annual International Conference and Exhibition, Lagos, Nigeria, 5-7 August. SPE-167568.

Odusina, E. O., Sondergeld, C. H., and Rai, C. S. 2011. NMR Study of Shale Wettability. Presented at the Canadian Unconventional Resources Conference, Calgary, Alberta, Canada, 15-17 November. SPE-147371-MS.

Oklahoma Oil and Gas Association, 2017, Economic Timeline of Drilling an Oil and Gas Well in Oklahoma, 26 April, 2017, http://okoga.com/wp-content/uploads/2017/05/OK-Oil-Gas-Well-Drilling-OKOGA.pdf (accessed 11 November 2017)

Owens, W. W., Parrish, D. R., and Lamoreaux, W. E. 1956. An Evaluation of a Gas Drive Method for Determining Relative Permeability Relationships. Petroleum Transactions, AIME **207**: 275-280.

Passey, Q. R., Bohacs, K., Esch, W. L., Klimentidis, R. and Sinha, S. 2010. From Oil-Prone Source Rock to Gas-Producing Shale Reservoir - Geologic and Petrophysical Characterization of Unconventional Shale Gas Reservoirs. Presented at the International Oil and Gas Conference and Exhibition, Beijing, China, 8-10 June. SPE-131350-MS.

Pittman, E. 1992. Relationship of Porosity and Permeability to Various Parameters Derived From Mercury Injection-Capillary Pressure Curves for Sandstones. AAPG Bulletin, V.76, 1992, p. 191-198.

Profice, S., Lasseux, D., Jannot, Y., Jebara, N., and Hamon, G. 2012. Permeability, Porosity and Klinkenberg Coefficient Determination on Crushed Porous Media. Petrophysics, **53** (6): 430-438.

Ross, D. J., and Bustin, R. M. 2009. The Importance of Shale Composition and Pore Structure Upon Gas Storage Potential of Shale Gas Reservoirs. Marine and Petroleum Geology, **26**: 916-927.

Roth, M. 2011. North American Shale Gas Reservoirs: Similar, Yet so Different. American Association of Petroleum Geologists Convention, Calgary. Search Discov Art #80136

Sakhaee-Pour, A., and Bryant, S. 2012. Gas Permeability of Shale. SPE Reservoir Evaluation and Engineering, **15**(4): 401-409.

Sinha, S., Braun, E. M., Determan, M. D., Passey, Q. R., Leonardi, S. A., Boros, J. A., Wood III, A. C., Zirkle and T. Kudva, R. A. 2012. Advances in Measurement Standards and Flow Properties Measurements for Tight Rocks Such as Shales. Presented at SPE/EAGE European Unconventional resources Conference and Exhibition, Vienna, Austria, 20–22 March. SPE–152257-MS.

Sinha, S., Braun, E. M., Determan, M. D., Passey, Q. R., Leonardi, S. A., Boros, J. A., and Kudva, R. A. 2013. Steady-State Permeability Measurements on Intact Shale Samples at Reservoir Conditions - Effect of Stress, Temperature, Pressure, and Type of Gas. Presented at the SPE Middle East Oil and Gas Show and Conference, Manama, Bahrain, 10-13 March. SPE-164263-MS.

Sondergeld, C. H., Newsham, K. E., Comisky, J. T., Rice, M. C., and Rai, C. S. 2010. Petrophysical Considerations in Evaluating and Producing Shale Gas Resources, Presented at SPE Unconventional Gas Conference, Pittsburgh, Pennsylvania, 23-25 February. SPE-131768-MS.

Swanson, B. F. 1981. A Simple Correlation Between Permeability and Mercury Capillary Pressures, JPT **27**: 2498-2504.

Taking Center Stage, Reprinted from Oilfield Technology, February 2013, https://www.slb.com/~/media/Files/completions/industry_articles/201302_ot_taking_centre_stage_bakken_ia.pdf (accessed 11 November 2017)

Tinni, A., Fathi, E., Agarwal, R., Sondergeld, C. H., Akkutlu, I. Y. and Rai, C. S. 2012. Shale Permeability Measurements on Plugs and Crushed Samples. Presented at the SPE Canadian Unconventional Resources Conference, Calgary, Alberta, Canada. 30 October-1 November. SPE-162235-MS.

Tinni, A., Odusina, E., Sulucarnain, I., Sondergeld, C., and Rai, C. 2014. NMR Response of Brine, Oil and Methane in Organic Rich Shales. Presented at SPE Unconventional Resources Conference, The Woodlands, Texas, 1-3 April. SPE-168971-MS.

Thomeer, J. H. M. 1960. Introduction of a Pore Geometrical Factor Defined by the Capillary Pressure Curve. Trans., AIME: 73- 77.

Thomeer J. H. M. 1983. Air Permeability as a Function of Three Pore Network Parameters. Trans., AIME: 809-814.

Wang, R., Zhang, K., Detpunyawat, P., Cao, J., and Zhan, J. 2016. Analytical Solution of Matrix Permeability of Organic-Rich Shale. Presented at the International Petroleum Technology Conference, Bangkok, Thailand, 14-16 November. IPTC-18627-MS.

Wasaki, A., and Akkutlu, I. Y. 2015. Permeability of Organic-Rich Shale. SPE Journal **20** (6). SPE-170830-PA.

Wattenbarger, R. A., El-Banbi, A. H., Villegas, M. E., and Maggard, J. B. 1998. Production Analysis of Linear Flow into Fractured Tight Gas Wells. Presented at SPE Rocky Mountain Regional/Low-Permeability Reservoirs Symposium, Denver, Colorado, 5-8 April. SPE-39931-MS.

Yang, D., Elsworth, D., Kang, Z. Q., Zhao, Y. S., and Zheng, B. S. 2012. Experiments on Permeability Evolution with Temperature of Oil Shale. Presented at the 46th US Rock Mechanics/Geomechanics Symposium, Chicago, Illinois, 24-27 June. ARMA-2012-386.

Zheng, D., 2016, Integrated Production Data Analysis of Horizontal Fractured Well in Unconventional Reservoir. MS thesis, University of Oklahoma, Norman, Oklahoma. (2016)